Modeling pinchoff and reconnection in a Hele-Shaw cell. I. The models and their calibration

Hyeong-Gi Lee and J. S. Lowengrub[a]
School of Mathematics, University of Minnesota, Minneapolis, Minnesota 55455

J. Goodman
Courant Institute of Mathematical Sciences, New York University, New York, New York 10012

This is the first paper in a two-part series in which we analyze two model systems to study pinchoff and reconnection in binary fluid flow in a Hele-Shaw cell with arbitrary density and viscosity contrast between the components. The systems stem from a simplification of a general system of equations governing the motion of a binary fluid (NSCH model [Lowengrub and Truskinovsky, Proc. R. Soc. London, Ser. A **454**, 2617 (1998)]) to flow in a Hele-Shaw cell. The system takes into account the chemical diffusivity between different components of a fluid mixture and the reactive stresses induced by inhomogeneity. In one of the systems we consider (HSCH), the binary fluid may be compressible due to diffusion. In the other system (BHSCH), a Boussinesq approximation is used and the fluid is incompressible. In this paper, we motivate, present and calibrate the HSCH/BHSCH equations so as to yield the classical sharp interface model as a limiting case. We then analyze their equilibria, one dimensional evolution and linear stability. In the second paper [paper II, Phys. Fluids **14**, 514 (2002)], we analyze the behavior of the models in the fully nonlinear regime. In the BHSCH system, the equilibrium concentration profile is obtained using the classical Maxwell construction [Rowlinson and Widom, *Molecular Theory of Capillarity* (Clarendon, Oxford, 1979)] and does not depend on the orientation of the gravitational field. We find that the equilibria in the HSCH model are somewhat surprising as the gravitational field actually affects the internal structure of an isolated interface by driving additional stratification of light and heavy fluids over that predicted in the Boussinesq case. A comparison of the linear growth rates indicates that the HSCH system is slightly more diffusive than the BHSCH system. In both, linear convergence to the sharp interface growth rates is observed in a parameter controlling the interface thickness. In addition, we identify the effect that each of the parameters, in the HSCH/BHSCH models, has on the linear growth rates. We then show how this analysis may be used to suggest a set of modified parameters which, when used in the HSCH/BHSCH systems, yield improved agreement with the sharp interface model at a finite interface thickness. Evidence of this improved agreement may be found in paper II. © *2002 American Institute of Physics.* [DOI: 10.1063/1.1425843]

I. INTRODUCTION

This is the first paper in a two-part series in which we analyze two model systems to study pinchoff and reconnection in binary fluid flow in a Hele-Shaw cell with arbitrary density and viscosity contrast between the components. The systems stem from a simplification of a general system of equations governing the motion of a binary fluid (NSCH model[1]) to flow in a Hele-Shaw cell. The system takes into account the chemical diffusivity between different components of a fluid mixture and the reactive stresses induced by inhomogeneity. Our goal is to investigate these effects on flow, and in particular through pinchoff and reconnection of interfaces, in a simpler setting than the general system. In addition to the intrinsic interest of analyzing these effects in

a binary Hele-Shaw flow, one of the goals of this paper is develop insight that can be used in an analysis of the full NSCH model.

In this paper, we motivate, present and calibrate the equations so as to yield the classical sharp interface model as a limiting case. We then analyze their equilibria, one-dimensional evolution and linear stability. In the second paper (paper II[2]), we analyze the behavior of the models in the fully nonlinear regime though pinchoff and reconnection.

A Hele-Shaw cell consists of two flat parallel plates separated by a small gap b, see Fig. 1, and between the plates there is viscous fluid.[3] The cell was originally designed by Hele-Shaw[4] to study two-dimensional potential flow. Recently, there has been much interest in Hele-Shaw flows largely because the gap-averaged velocity of the fluid is given by Darcy's law and is identical to that of a fluid moving through a porous medium with permeability $b^2/12$, see, for example, Refs. 5–7. In addition, the relative simplicity of the equations of motion also makes Hele-Shaw flows ideal

---

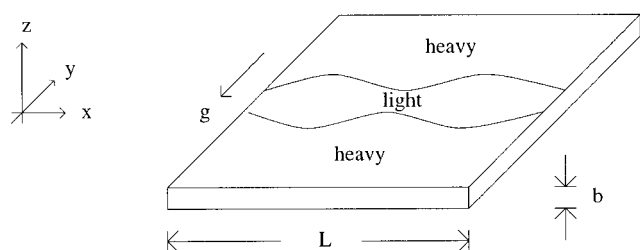[a]Also in Department of Chemical Engineering and Materials Science, University of Minesota.

FIG. 1. A Hele-Shaw cell in which light and heavy fluids are separated by interfaces (Ref. 3).

test cases in which to develop mathematical theory and numerical methods to study singularities and topological transitions, see for instance Refs. 8–17. The latter is our point of view here.

Topological transitions such as pinchoff and reconnection of interfaces are fundamental features of multicomponent fluid flows. The details of such transitions are important in many physical processes as mixing and reaction rates may sensitively depend on the production/reduction of interfacial area. In general, the dynamics of topological transitions are difficult to understand and model even in the Hele-Shaw context. It is not obvious how to change the interface topology in a physically justified manner using continuum theory and numerical simulation. The collision of material surfaces, for instance, produces a singularity in the fluid equations (e.g., see Ref. 18).

In interface tracking algorithms for example (e.g., Refs. 19–26), *ad hoc* cut-and-connect procedures are typically used to change the topology of interfaces. Only in a few special cases involving liquid/air interfaces is it possible to develop physically based reconnection conditions based on similiarity solutions of the fluid equations.[27–29] The development of such similarity solutions and reconnection conditions for the general liquid/liquid case remains open and thus it is difficult to provide a physical justification for the cut-and-connect rules. In fact, in the context of colliding drops, Nobari *et al.*[24] noticed that the flow may sensitively depend on the time at which the interface surgery is performed.

In interface capturing algorithms, such as color function and level set methods (e.g., see Refs. 30–35), and the volume of fluid method (also sometimes referred to as a tracking method, e.g., see Refs. 36–40) an analogous ambiguity arises. In these methods, the fluid equations are augmented with an additional conservation law for the color/level set function and volume fraction, respectively, which are used to mark each fluid domain. The numerical viscosity introduced by using an upwind method to solve the equations of motion actually allows topological transitions to occur smoothly. The flow discontinuities (density, viscosity) are typically smoothed as well although there are now several methods in which the interface jump conditions (i.e., surface tension) are handled explicitly.[41–43] It is not clear, however, which types of smoothing and numerical viscosity are physically justified.

Recently, Goodman, Lowengrub, and Shelley[44] suggested that chemical diffusion between the different fluid components provides a physical mechanism to smooth flow discontinuities and to yield smooth evolutions through topology changes. They gave a physical derivation of the equations for binary fluids with density matched, or nearly density matched, components (also known as model H,[45] see below). The diffusion is limited if the components are macroscopically immiscible and reflects the partial miscibility real fluids always display. As a consequence, interfaces separating the flow components are diffuse although the thickness of interfaces between real immiscible fluids, such as oil and water, may be microscopic in many circumstances. The interface thickness and structure may be important at topological transitions since the distance between interfaces becomes comparable to the interface thickness.

With topology transitions in mind, Lowengrub and Truskinovsky[1] gave a systematic derivation of the general equations governing the motion of a binary fluid. In this model, subsequently referred to as the NSCH model, the mass concentration is coupled to the fluid motion and the resulting system couples the Navier–Stokes (NS) equations to a nonlinear, fourth order diffusion equation of Cahn–Hilliard (CH, Ref. 46) type for the concentration. The gradients in concentration produce reactive stresses in the fluid which mimic surface tension. The NSCH model reduces to a system known as model H[45] (see also Refs. 47 and 48) when the flow components are density matched. When the components have different densities, diffusion may create density variation and in the NSCH model, the binary fluid may be slightly compressible even if the components are incompressible, e.g., see Joseph[49] and Perera and Sekerka.[50] Moreover, the chemical potential depends explicitly on the fluid pressure. We note that Antanovskii[51] also derived equations for the motion of a binary fluid with immiscible components with different densities. His system shares common features with the NSCH model however the dependence of the chemical potential upon the pressure is missing.

The idea that interfaces have a finite thickness dates to Poisson,[52] Gibbs,[53] Rayleigh,[54] van der Waals,[55] and Korteweg.[56] The idea is according to the thermodynamics of immiscible fluids, there is a range of concentrations (of one of the components) where the free energy is concave and homogeneous states are unstable.[53] An interface between two immiscible fluids may then be described as a layer where thermodynamically unstable mixtures are stabilized by weakly nonlocal terms (gradients) in the energy[55] which have their origins in molecular force interactions between the components.[3,57] These gradient terms induce extra reactive stresses in the fluid which become surface stress in the zero thickness limit.[58]

There has been much recent work on the use of diffuse interfaces in multicomponent fluid flows. Applications include modeling the two- and three-dimensional Rayleigh–Taylor instability (e.g., Refs. 59, 63, and 44), the pinchoff of liquid/liquid jets (e.g., Ref. 38), thermocapillary flow (e.g., Refs. 60 and 61), mixing (e.g., Ref. 62), contact angles and wetting phenomena (e.g., Refs. 63 and 64), nucleation and spinodal decomposition (e.g., Refs. 65, 66, 38, 60, and 61), gravity and capillary waves (e.g., Refs. 67–69), coalescence (e.g., Ref. 61), reactive flows [e.g., Struchtrup and Dold (pre-

print)] and the displacement of miscible fluids (e.g., Refs. 70, 49, 71, and 72). In the interest of brevity, we have cited only a few works. We refer the interested reader to the review of recent research by Anderson, McFadden, and Wheeler[73] and the references contained therein for a much more complete listing.

In this paper, we use a simplified NSCH model to study binary fluid flow in a Hele-Shaw (HS) cell. In particular, we follow the classical sharp interface model and assume Poiseuille flow between the plates. In addition, we assume there is no diffusion in the direction normal to the plates. This results in a generalized Darcy law in which there is only planar flow and diffusion. This yields one of the simplest such systems that can describe the flow and indeed captures topological transitions smoothly (referred to as the HSCH model). However, it does not account for 3D flow which could play a role near the meniscus and near pinchoff and reconnection. To rule out such effects, one would have to perform a detailed analysis of meniscus region as is done by Park and Homsy[74] for the classical Hele-Shaw model. We do not present such an analysis here (although it seems quite possible such an analysis could be performed at least away from topology transitions) and thus our model should be understood as just that—a model. We do provide an indirect justification for our model by demonstrating that it converges to the classical sharp interface models in the limit of zero interface thickness.

In this work, we consider primarily buoyancy driven flow (Rayleigh–Taylor instability) in which the two components are incompressible and macroscopically immiscible. The densities of the fluids may be arbitrary but the viscosities must be nonvanishing. We also consider a Boussinesq limit (referred to as the BHSCH model) in which density variation is assumed to non-negligible only in the gravitational force. The HSCH and BHSCH models are calibrated so that the classical sharp interface model is a limiting case; we note that other nonclassical sharp interface limits are possible.[1] Several essential features of the NSCH system are retained in the HSCH model including the reactive stresses, the diffusionally induced compressibility and the pressure dependence of the chemical potential. The BHSCH model contains reactive stresses but the flow is incompressible and the chemical potential does not depend on the pressure since density variation is assumed to be small. Thus, Hele-Shaw flow provides a simpler setting than the full NSCH model in which to compare and contrast these effects.

Recently, E and Palffy-Muhoray[75] derived equations similar to the HSCH model to study polymer melts (see also Ref. 76). In addition, Verschueren[61] derived an analogous system to study thermocapillary flow in a Hele-Shaw cell. In the case of density matched components, the HSCH model reduces to one which was previously used by Shinozaki and Oono[77] to study spinodal decomposition and has been recently used by Verschueren[61] to study coalescence in hyperbolic flows. We note that very recently, Struchtrup and Dold (preprint) derived a version of the HSCH system to study miscible, buoyantly unstable reaction fronts in a Hele-Shaw cell.

The HSCH and BHSCH models belong collectively to the class of phase-field models which have been widely used for free boundary problems in other physical situations such as the solidification of binary alloys, e.g., see the review edited by Gurtin and McFadden.[78] In fact, because there is a close connection between quasisteady diffusion and the Hele-Shaw problem (both involve harmonic fields in a domain with a free boundary), some phase-field equations (even the classical Cahn–Hilliard equation), have Hele-Shaw like sharp interface limits (e.g., Refs. 79–82). Typically these limiting models do not include hydrodynamic effects such as buoyancy. Very recently, however, Folch et al.[83] derived, analyzed, and implemented numerically a phase-field model for Hele-Shaw flows, with buoyancy and arbitrary viscosity contrast, to study the evolution of viscous fingers (e.g., Ref. 84). They also consider only planar flow. However, their approach differs from ours in several important ways. In their model, a modified Allen–Cahn equation[85] (nonconservative equation) governs the motion of the phase field which is then coupled to a dissipative, time evolution equation for the stream function. Although Folch et al. show that this system converges to the classical Hele-Shaw system in the thin interface limit and indeed reproduces fingering, it seems difficult to justify their choice of phase-field function and governing equations from physical considerations. Our approach, on the other hand, is motivated by physical considerations such as chemical diffusion between the liquid components.

In this paper, the differences between the HSCH, the BHSCH and sharp interface models are studied by considering equilibrium solutions and their linear stability. In the BHSCH system, the equilibrium concentration profile is obtained using the classical Maxwell construction[3] and does not depend on the orientation of the gravitational field. In the HSCH system, on the other hand, the gravitational field actually affects the internal structure of an isolated interface by driving additional stratification of light and heavy fluids over that predicted in the Boussinesq case. We are only able to obtain an equilibrium solution numerically for the stably stratified case and there is no analytic formula. Boundary layers in the equilibrium solution are observed and the evolution towards the stably stratified equilibrium simulated in one dimension. It remains an open question as to whether an unstably stratified equilibrium solution of the HSCH model exists.

The linear stability of unstably stratified equilibria to two-dimensional perturbations is studied using two approaches. In the first, the linearized equations are solved directly in the BHSCH context using an analytic formula for the equilibrium concentration profile. Because no such formula exists for the HSCH case, a practical comparison is made between the growth rates for the two models by solving the full equations numerically in the linear regime. The BHSCH and HSCH growth rates are consistent although the HSCH system is seen to be slightly more diffusive than the BHSCH system. Linear convergence to the sharp interface growth rates is observed in a parameter controlling the interface thickness. In addition, we identify the effect that each of the parameters, in the HSCH/BHSCH models, has on the linear growth rates. We then use this information to suggest a

modified set of parameters for which a better match is obtained between the HSCH/BHSCH and sharp interface linear growth rates at finite interface thicknesses. The models with the modified parameters still have the sharp interface model as a limiting case. In paper II, we present evidence indicating that improved agreement between the models is achieved in the nonlinear regime as well. This technique of enhancing agreement is quite general and has application beyond the current context.

The outline of the paper is as follows. In Sec. II, we present a derivation of the HSCH and BHSCH models. In Sec. III, the method of matched asymptotic expansions is used to obtain the sharp interface limit of the models. In Sec. IV, the equilibrium solutions of the models are given and, in addition, the evolution (one dimensional) is studied for the HSCH system. In Sec. V, the linear stability of the equilibrium solutions is analyzed. Last, in Sec. VI, conclusions are given.

II. THE HELE-SHAW–CAHN–HILLIARD MODEL

Consider a viscous two-component (binary) fluid between two parallel plates with gap width b. We suppose that the two plates are located at $z = \pm b$ and extend over the region $0 \leq x, y \leq L$ where $\delta = b/L$ is small. See Fig. 1 for an illustration of a Hele-Shaw cell with a layer of light fluid surrounded by heavy fluid. Let us begin by considering the classical sharp interface model.

A. Classical sharp interface model

In the classical sharp interface model,[84] Darcy's law is assumed to hold in each fluid

$$\nabla \cdot \mathbf{u}_i = 0, \tag{2.1}$$

$$\mathbf{u}_i = -\frac{1}{12\eta_i}(\nabla p_i - \tilde{G}\rho_i \mathbf{g}), \tag{2.2}$$

where $i = 1$, 2 denotes the fluid region, $\mathbf{u}_i$ denotes the gap-averaged fluid velocity, η_i is the viscosity, p_i is the pressure, ρ_i is the density, $\tilde{G}$ is the gravitational force in the direction of the unit vector $\mathbf{g} = \mathbf{e}_2 = (0,1)$. In addition, we have absorbed the effect of gap width into the velocity scale and the above equations have been made nondimensional using a characteristic velocity scale U^*, pressure scale p^*, density scale ρ^*, viscosity scale η^*, gravitational scale G, and length scale L.

If the fluid components are immiscible, a sharp interface Γ separates them. The boundary conditions on the interface Γ are assumed to be

$$(\mathbf{u}_1 - \mathbf{u}_2) \cdot \mathbf{n} = 0, \tag{2.3}$$

$$(p_2 - p_1) = \tau\kappa, \tag{2.4}$$

where $\mathbf{n}$ is the unit normal vector to Γ, κ is the curvature, and τ is the dimensionless surface tension coefficient. In the cases we will consider in this paper, the flow is characterized by the two relevant physical parameters

$$\mathbf{B} = \tilde{G}(\rho_2 - \rho_1)/\tau \quad \text{the Bond number}, \tag{2.5}$$

which measures the relative strengths of the gravitational and surface tension forces. For example, in Fig. 1, the upper interface has $\mathbf{B} < 0$ (unstable stratification) while the lower interface has $\mathbf{B} > 0$ (stable stratification). In addition, let

$$\mathbf{A} = \frac{\eta_1 - \eta_2}{\eta_1 + \eta_2} \quad \text{be the Atwood number}, \tag{2.6}$$

which is a measure of the difference in the fluid components' viscosity.

The system (2.1)–(2.4) is dissipative. This is seen most easily in the case of zero gravity where the system energy is just the surface energy

$$E(t) = \int_\Gamma \tau \, ds \tag{2.7}$$

that is dissipated at the rate

$$\dot{E}(t) = -12 \sum_{i=1}^{2} \eta_i \int_{\Omega_i} |\mathbf{u}_i|^2 \, dA. \tag{2.8}$$

Before turning to the Hele-Shaw–Cahn–Hilliard system, a few remarks are in order. In a certain sense, the sharp interface system given above represents the simplest set of equations governing the motion of a viscous fluid between two closely spaced parallel plates.[84] The system is obtained from the Navier–Stokes equations by assuming that the viscous forces dominate the inertial forces and that the bulk flow between the plates is Poiseuille flow. However, because the flow may actually be fully three dimensional in the region near the two-fluid interface Γ, particularly near the glass plates due to flow near the contact region, it is not at all obvious that Darcy's law in fact holds near Γ. Further, Γ actually has two-dimensional curvature so that it is also not clear that the pressure jump condition (2.4) holds across Γ. Nevertheless, under several assumptions, including that of complete wetting of the plates by the displaced fluid, Park and Homsy[74] performed a matched asymptotic analysis near Γ and showed that for small capillary numbers, the above system indeed describes the leading order behavior of the flow provided that the surface tension τ is appropriately modified. We wish to make this point because in the Hele-Shaw–Cahn–Hilliard models we present next, we also assume Poiseuille flow and neglect three-dimensional diffusion near the interface and contact region.

B. The Navier–Stokes–Cahn–Hilliard model

The Hele-Shaw–Cahn–Hilliard models we consider in this paper are versions of the general Navier–Stokes–Cahn–Hilliard (NSCH) model (see Ref. 1), simplified to model the Hele-Shaw geometry. For completeness, we briefly review the NSCH model. In this model, a mass concentration field $c(\mathbf{x},t)$ is introduced to denote the mass ratio of one of the components in a heterogeneous mixture of two fluids (e.g., M_1/M where M_1 is the mass of component 1 and M is the total mass of the binary fluid in a representative volume V). In this paper, c is always taken to be the mass concentration of the fluid labeled 1.

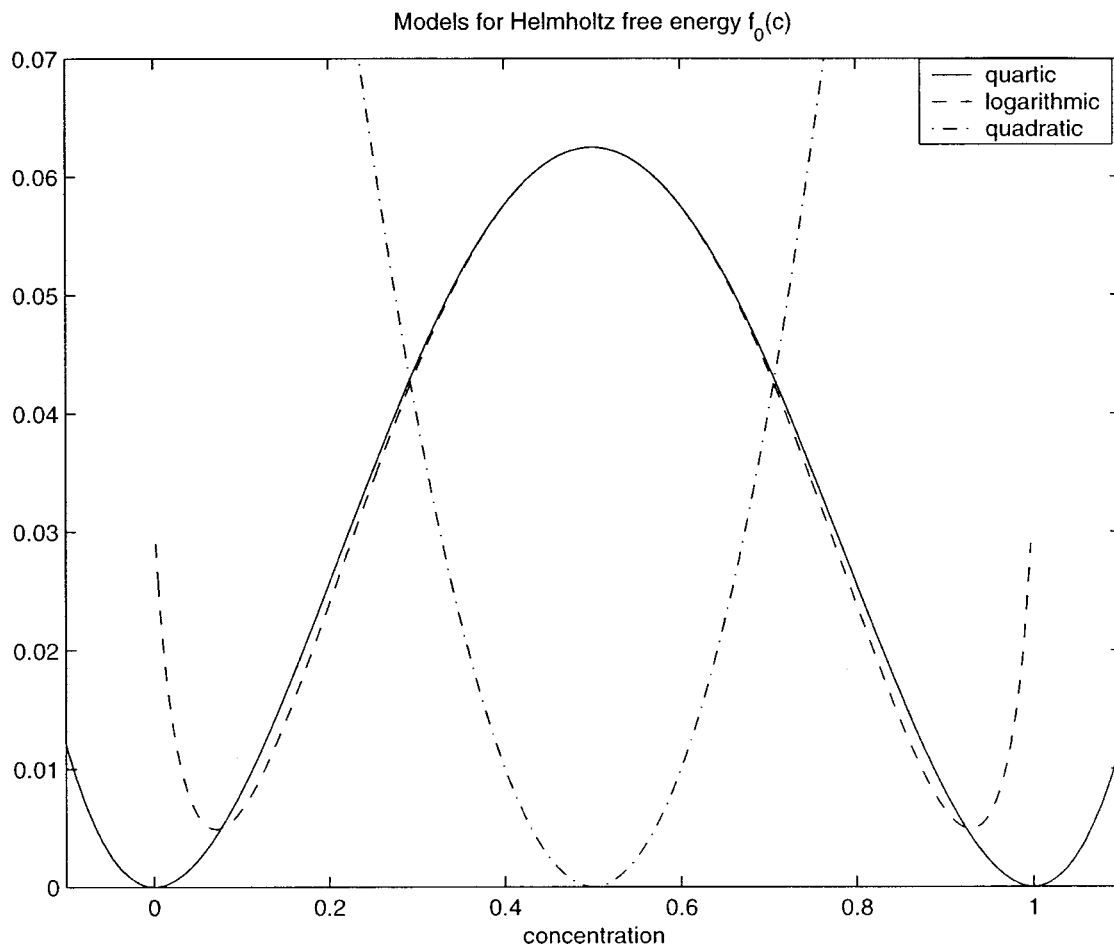Models for Helmholtz free energy f_0(c)

FIG. 2. Illustration of models for $f_0(c)$ for immiscible and miscible fluids. Solid curve, quartic free energy, $f_0(c) = c^2(1-c)^2$; dashed curve, logarithmic free energy, $f_0(c) = 0.5[c \log(c) + (1-c)\log(1-c)] - 0.75[c^2 + (1-c)^2] + 0.7841$; dotted–dashed curve, $f_0(c) = (c-0.5)^2$.

As an illustrative example, let component 1 be oil, component 2 be water and thus the binary fluid is the combination of the two (separated by very thin interfaces). Even though such a combination of fluids is macroscopically immiscible, there is nevertheless a narrow region of chemical mixing in which van der Waals (intermolecular) forces play an important role.[53,55]

Separately, the fluid components are assumed to be incompressible and have constant densities and viscosities. We assume that the density of the binary fluid depends on the concentration but not on the pressure. This is referred to as the "quasi-incompressible" case[1] since diffusion may introduce density variation and hence may cause the binary fluid to be slightly compressible. Diffusion is allowed to occur between the fluid components which is limited if the components are macroscopically immiscible.

Let ρ_1, ρ_2 and $\mathbf{v}_1, \mathbf{v}_2$ be the densities (M_i/V) and velocities of the two fluid components, respectively. Let $\rho = \rho(c)$ be the total density (M/V) and $\mathbf{v}$ be the mass-averaged velocity field, i.e., $\rho\mathbf{v} = \rho_1\mathbf{v}_1 + \rho_2\mathbf{v}_2$. Then, in dimensional form, the NSCH equations are

$$\nabla \cdot \mathbf{v} = -\frac{\rho'(c)}{\rho}\dot{c}, \tag{2.9}$$

$$\rho\dot{\mathbf{v}} = -\nabla p - \epsilon\nabla \cdot (\rho\nabla c \otimes \nabla c) + \rho\mathbf{G}$$
$$+ \nabla \cdot (\eta(\nabla\mathbf{v} + \nabla\mathbf{v}^T)) + \nabla(\lambda\nabla \cdot \mathbf{v}), \tag{2.10}$$

$$\rho\dot{c} = \nabla \cdot (\nu\nabla\mu), \tag{2.11}$$

where $\cdot = \partial_t + \mathbf{v}\cdot\nabla$ is the advective derivative, $\rho = \rho(c)$ is the density, $\mathbf{v} = (u,v,w)$ is the velocity, p is the pressure, λ and η are the viscosity coefficients, $\mathbf{G} = -\nabla\Phi$, Φ is the gravitational potential, and ' denotes the derivative with respect to c. μ is the generalized chemical potential given by

$$\mu = f_0'(c) - \frac{\rho'(c)}{\rho^2}[p - (\lambda + 2\eta/3)\nabla \cdot \mathbf{v}] - \frac{\epsilon}{\rho}\nabla \cdot (\rho\nabla c), \tag{2.12}$$

where $f_0(c)$ is the Helmholtz free energy. Note that the chemical potential depends explicitly on the fluid pressure and the bulk viscosity. This form of μ is slightly more general than that presented in Ref. 1 since it was assumed there that the bulk viscosity was equal to zero. The derivation of Eq. (2.12) follows straightforwardly from the approach given in Ref. 1.

If the fluid components are immiscible, then f_0 is taken to be a nonconvex function of c. If the components are miscible, f_0 is taken to be a convex function of c. See Fig. 2.

Note that for f_0 nonconvex, there is a region (called the spinodal region) in which the diffusion coefficient $f_0''(c)$ <0. This creates antidiffusion and is what prevents the fluids from mixing completely.

Finally, the two additional parameters ϵ and ν may be interpreted as follows. ϵ is a measure of nonlocality (gradient energy) which, as we will see, effectively introduces an internal length scale (interface thickness in the immiscible case), see Refs. 46 and 1 for example. ν is a measure of nonviscous dissipation and may also be interpreted as a mobility.

We wish to point out two important features of the NSCH model. First, the velocity $\mathbf{u}$ is not necessary solenoidal which may introduce compressibility effects. Second, gradients in concentration may produce stresses which as we see in the next section, mimic the effect of surface tension. For further details, we refer the reader to Ref. 1.

Equations (2.9)–(2.11) have the associated energy functional

$$E=\int_\Omega \rho\left[\frac{|\mathbf{v}|^2}{2}+f_0(c)+\frac{\epsilon}{2}|\boldsymbol{\nabla}c|^2+\Phi\right]dx\,dy\,dz, \quad (2.13)$$

which is the sum of the kinetic, surface (chemical) and potential energies. It is easily seen that

$$\dot{E}=-\int_\Omega \nu|\boldsymbol{\nabla}\mu|^2\,dx\,dy\,dz-\int_\Omega\left[\eta\sum_{i=1}^3|\boldsymbol{\nabla}v_i|^2\right.$$

$$\left.+(\eta+\lambda)(\boldsymbol{\nabla}\cdot\mathbf{v})^2\right]dx\,dy\,dz+\text{boundary terms.}$$

$$(2.14)$$

We further assume that the viscosity coefficients η and λ may depend on c and that ϵ and ν are constant.

On the parallel plates, we take the boundary conditions

$$\mathbf{v}=0, \quad \text{no slip}, \tag{2.15}$$

$$c_z=0, \quad \text{no concentration flux}, \tag{2.16}$$

$$\mu_z=0, \quad \text{no diffusion flux}, \tag{2.17}$$

at $z=\pm b/2$, where the subscript z denotes $\partial/\partial z$. We note that Eqs. (2.16) and (2.17) imply that the liquid/solid contact angle is 90°. We choose these boundary conditions for simplicity. See Jacqmin[63] for a discussion of other concentration boundary conditions and their relation to liquid/solid contact angles.

C. Simplification of the NSCH model for flow in a Hele-Shaw cell

Next, we obtain the Hele-Shaw–Cahn–Hilliard system by supposing in the NSCH model that the viscous forces dominate the inertial forces, the flow between the plates is Poiseuille flow and that there is no diffusion in the z direction so that c is independent of z. Using an analogous nondimensionalization as in the sharp interface case, the HSCH model is given as

HSCH model

$$\boldsymbol{\nabla}\cdot\mathbf{u}=-\frac{1}{\rho}\rho'(c)(c_t+\mathbf{u}\cdot\boldsymbol{\nabla}c)=-\frac{\rho'}{\rho^2}\frac{1}{\mathbf{Pe}}\Delta\mu, \tag{2.18}$$

$$\mathbf{u}=-\frac{1}{12\eta(c)}\left[\boldsymbol{\nabla}p+\frac{\mathbf{C}}{\mathbf{M}}\boldsymbol{\nabla}\cdot(\rho\boldsymbol{\nabla}c\otimes\boldsymbol{\nabla}c)-\widetilde{G}\rho\mathbf{g}\right], \tag{2.19}$$

$$\rho(c_t+\mathbf{u}\cdot\boldsymbol{\nabla}c)=\frac{1}{\mathbf{Pe}}\Delta\mu, \tag{2.20}$$

where $\mathbf{Pe}=U^*\rho^*L/(\nu\mu^*)$ is the diffusional Peclet number (μ^* is a characteristic scale of $f_0'(c)$), $\mathbf{C}=\epsilon/(\mu_*L)$ is the Cahn number (a measure of interface thickness), and $\mathbf{M}=p^*/(\rho^*\mu^*)$ is a Mach number (a measure of the relative strengths of the pressure and chemical forces). $\boldsymbol{\nabla}$ and Δ denote the two-dimensional gradient and Laplace operators. The generalized chemical potential μ is given by

$$\mu=f_0'(c)-\mathbf{M}\frac{\rho'(c)}{\rho^2}p-\mathbf{C}\frac{1}{\rho}\boldsymbol{\nabla}\cdot(\rho\boldsymbol{\nabla}c). \tag{2.21}$$

The dimensionless energy for the HSCH equations can be obtained by dropping the kinetic energy and nondimensionalizing the NSCH energy in Eq. (2.13) to yield

$$E=\frac{1}{\mathbf{M}}\int_{\Omega_2}\rho(c)\left[\left(f_0(c)+\frac{\mathbf{C}}{2}|\boldsymbol{\nabla}c|^2\right)+\mathbf{M}\widetilde{G}\Phi\right]dx\,dy, \tag{2.22}$$

which is the sum of the dimensionless surface (chemical) and potential energies. By Ω_2, we denote the reduced two-dimensional domain. It is not difficult to see that the energy is dissipated by the evolution

$$\dot{E}(t)=-\int_{\Omega_2}12\eta|\mathbf{u}|^2\,dx\,dy-\frac{1}{\mathbf{M}}\int_{\Omega_2}\frac{1}{\mathbf{Pe}}|\boldsymbol{\nabla}\mu|^2\,dx\,dy$$

$$+\frac{1}{\mathbf{M}}\int_{\partial\Omega_2}\mathbf{C}\rho c_t\partial_n c+\frac{1}{\mathbf{Pe}}\mu\partial_n\mu-\left[\mathbf{M}q+\mathbf{M}\widetilde{G}\rho\Phi\right.$$

$$\left.+\rho\left(f(c)-\frac{\mathbf{C}}{2}|\boldsymbol{\nabla}c|^2\right)\right]\mathbf{u}\cdot\mathbf{n}\,dS. \tag{2.23}$$

This is one of the simplest diffusional systems that can describe binary Hele-Shaw flow and is in the spirit of the sharp interface model presented earlier. However, it does neglect three-dimensional flow and diffusion which could play a role near the meniscus, pinchoff and reconnection. While we do not present an analogous version of the analysis of Park and Homsy to justify our assumptions, it seems quite possible that such an analysis could be performed, at least away from topology transitions. We do provide an indirect justification for the HSCH model by demonstrating that it converges to the classical sharp interface models in the limit of zero interface thickness.

The HSCH model is considerably simpler than the NSCH system. As such, it provides a simpler forum in which to investigate the effects of diffusion and compressibility on the fluid motion. We note that equations similar to (2.18)–(2.21) were derived by E and Palffy-Muhoray in the context of polymer melts.[75] In particular, those authors noticed the dependence of the chemical potential on the pressure. However, they did not seem to account for compressibility effects

due to density differences of the constituents. In addition, Verschueren derived an analogous system to study thermocapillary flow in a Hele-Shaw cell.[61] Very recently, Struchtrup and Dold (preprint) derived a version of the HSCH system to study miscible, buoyantly unstable reaction fronts in a Hele-Shaw cell.

Finally, we will take the following simple mixture model for the density in the HSCH system:

$$\frac{1}{\rho(c)} = \frac{1}{\rho_1} c + \frac{1}{\rho_2} (1-c), \tag{2.24}$$

where ρ_1 and ρ_2 are the nondimensional densities of two fluids before mixing. The formula (2.24) means that volume is preserved under mixing.[49] In the case of a simple mixture, the HSCH equations can be simplified by using

$$-\frac{\rho'(c)}{\rho^2} = \alpha \equiv \frac{1}{\rho_1} - \frac{1}{\rho_2}.$$

In this paper, we consider both the HSCH system given above and a slightly simpler version obtained from a Boussinesq approximation. To obtain this reduced system, we assume that the deviation between $\rho(c)$ and its spatial average $\langle\rho\rangle$ is small, but $[\rho(c) - \langle\rho\rangle]\widetilde{G}$ is not negligible. In the Boussinesq limit, we suppose that the density is a constant which we take equal to 1 everywhere except in the gravitational term. We refer to this simpler system as the BHSCH model and the equations are given by

BHSCH model

$$\nabla \cdot \mathbf{u} = 0, \tag{2.25}$$

$$\mathbf{u} = -\frac{1}{12\eta(c)} \left[\nabla p + \frac{\mathbf{C}}{\mathbf{M}} \nabla \cdot (\nabla c \otimes \nabla c) - \widetilde{G}\widetilde{\rho}(c)\mathbf{g} \right], \tag{2.26}$$

$$c_t + \mathbf{u} \cdot \nabla c = \frac{1}{\mathbf{Pe}} \nabla \mu, \tag{2.27}$$

where

$$\widetilde{\rho}(c) = (\rho_1 - 1)c + 1, \tag{2.28}$$

and $\rho_2 = 1$. Further,

$$\mu = f_0'(c) - \mathbf{C}\Delta c. \tag{2.29}$$

In the Boussinesq case, the energy Eq. (2.22) reduces to

$$E = \frac{1}{\mathbf{M}} \int \left[f_0(c) + \frac{\mathbf{C}}{2} |\nabla c|^2 + \mathbf{M}\widetilde{G}\widetilde{\rho}(c)\Phi \right] dx \, dy, \tag{2.30}$$

and a formula analogous to (2.23) may be obtained for $\dot{E}$ in the Boussinesq limit.

The BHSCH system is simpler than the HSCH model in that the velocity is solenoidal and the chemical potential does not depend directly on the fluid pressure. Concentration gradients still may produce nonzero velocities however. The system (2.25)–(2.27) has been used previously to study spinodal decomposition in a Hele-Shaw cell in the absence of gravity[77] and was recently used by Verschueren[61] to study coalescence in hyperbolic flows.

Before concluding this section, we rewrite the HSCH equations in a more useful way by using the vector identity

$$\nabla \cdot (\rho\nabla c \otimes \nabla c) = \nabla(\rho|\nabla c|^2) + \rho\Delta c\nabla c - \tfrac{1}{2}\nabla|\nabla c|^2$$

and introducing the modified pressure

$$q = p + \frac{\mathbf{C}}{\mathbf{M}} \rho|\nabla c|^2.$$

Using these, Eq. (2.19) can be written as

$$\mathbf{u} = -\frac{1}{12\eta(c)} \left[\nabla q + \frac{\mathbf{C}}{\mathbf{M}} \rho \left(\Delta c\nabla c - \frac{1}{2}\nabla|\nabla c|^2 \right) - \widetilde{G}\rho(c)\mathbf{g} \right], \tag{2.31}$$

and the chemical potential (2.21) may be written as

$$\mu = f_0'(c) - \frac{\rho'}{\rho^2}\mathbf{M}q - \mathbf{C}\Delta c. \tag{2.32}$$

Yet another equivalent form of Eq. (2.19) may be obtained by introducing the generalized Gibbs free energy

$$g = \frac{p}{\rho} + \frac{1}{2}\frac{\mathbf{C}}{\mathbf{M}}|\nabla c|^2 + \frac{1}{\mathbf{M}}f_0. \tag{2.33}$$

Using g, we obtain

$$\mathbf{u} = -\frac{\rho(c)}{12\eta(c)} \left[\nabla(g + \widetilde{G}\Phi) - \frac{1}{\mathbf{M}}\mu\nabla c \right]. \tag{2.34}$$

Using Eq. (2.34) we obtain a relatively simple form for the out of plane vorticity $\omega = \nabla \times \mathbf{u} \cdot \mathbf{e}_3$ where $\mathbf{e}_3$ is the unit vector out of the plane. The vorticity is given by

$$\omega = -\nabla\left(\frac{\rho(c)}{12\eta(c)}\right) \times \nabla(g + \widetilde{G}\Phi) \cdot \mathbf{e}_3$$

$$+ \frac{1}{\mathbf{M}}\nabla\left(\frac{\mu\rho(c)}{12\eta(c)}\right) \times \nabla c \cdot \mathbf{e}_3. \tag{2.35}$$

The first term on the right-hand side is the baroclinic vorticity and the second term is the vorticity due to surface tension.

III. THE SHARP INTERFACE LIMIT

In this section, we present the sharp interface limit of the HSCH model (2.18)–(2.21) away from topological transitions such as pinchoff and reconnections. To do this, we follow the approach in Ref. 1 and relate the **C**, **M**, and **Pe** numbers to a single parameter γ which measures the interface thickness:

$$\mathbf{C} = O(\gamma^2), \quad \mathbf{M} = O(\gamma), \quad \text{and} \quad \mathbf{Pe} = O(1/\gamma) \text{ or } O(1). \tag{3.1}$$

We then sketch matched asymptotic expansions in γ and show that at leading order in the outer equations, the classical sharp interface system is recovered. In addition, we show that the BHSCH model has the same classical leading order limit which suggests that for thin interfaces, the two approaches yield very similar results away from topology transitions. While this is indeed borne out by our numerical results in paper II,[2] we also note some important differences between the models. As we will see in the next section, there

are interesting differences in the 1D equilibria for the two models for finite γ. In particular, boundary layers are present in the HSCH equilibria and the gravitational field actually affects the concentration profile and hence the interface structure. Further, in paper II,[2] observe that the limiting behavior of the two models is subtly different near pinchoff and reconnection.

A. Sharp interface asymptotics

We now present a brief sketch of the matched asymptotic expansions of the HSCH and BHSCH systems. Following the standard approach (e.g., Pego[81]), we suppose that at time $t=0$, there is a single smooth transition layer of width $O(\gamma)$ separating two domains Ω_1 and Ω_2 where the fluids are nearly uniform. In particular, suppose that $c(\mathbf{x},0)=c_{1,2}+O(\gamma)$ in $\Omega_{1,2}$, respectively, where $c_{1,2}$ are the equilibrium concentrations of fluid 1 in the two domains [i.e., wells of the Helmholtz free energy $f_0(c)$]. Note that this implies $c_1 \approx 1$ and $c_2 \approx 0$. This initial condition for c is consistent with letting the fluids equilibrate before motion starts. Let Γ be a curve centered in the transition layer. The idea of the method is to expand c, $\mathbf{u}$ and p in powers of γ both away from the transition region (outer expansion, $\Omega_{1,2}$) and inside the transition region (inner expansion). In the inner expansion, a stretched local coordinate system (with respect to Γ) is used. In order for our expansions to be valid, the curvature κ of Γ must satisfy $\kappa \ll 1/\gamma$. By substituting these expansions into the equations and matching powers of γ, one can determine the field equations in the $\gamma \to 0$ limit. By matching the inner and outer expansions at the boundaries of the transition region, one can reconstruct the sharp interface jump conditions.

To be specific, we will take the scaling

$$\mathbf{C}=\gamma^2,$$

$$\mathbf{M}=\frac{\gamma}{\tau}\sqrt{2}\int_{c_2}^{c_1}\rho(c)\sqrt{f_0(c)-f_0(c_1)-f_0'(c_1)(c-c_1)}\,dc,$$

$$\mathbf{Pe}=1/\gamma \quad \text{or} \quad \mathbf{Pe}=1. \tag{3.2}$$

As will become apparent when we consider the inner expansion, this choice of $\mathbf{M}$ guarantees the sharp interface limit of the HSCH model, satisfies the Laplace jump condition (2.4) with the surface tension τ. In the BHSCH model, the ρ in $\mathbf{M}$ should be set to 1.

1. Outer expansions

In the outer domains Ω_1 and Ω_2, write the variables $\mathbf{u}$, c, and p as expansions in powers of γ:

$$\mathbf{u}(x,y,t)=\mathbf{u}^{(0)}(x,y,t)+\gamma\mathbf{u}^{(1)}(x,y,t)+\gamma^2\mathbf{u}^{(2)}(x,y,t)+\cdots,$$

$$c(x,y,t)=c^{(0)}(x,y,t)+\gamma c^{(1)}(x,y,t)+\gamma^2 c^{(2)}(x,y,t)+\cdots,$$

$$p(x,y,t)=\frac{1}{\gamma}p^{(-1)}(x,y,t)+p^{(0)}(x,y,t)+\gamma p^{(1)}(x,y,t)+\cdots.$$

The $1/\gamma$ term is introduced in the expansion for p for a reason to be explained when we discuss the inner expansion. Substituting the expansions into the HSCH equations (2.18)–(2.21), the leading order equations are

$$\nabla p^{(-1)}=0, \tag{3.3}$$

$$\mathbf{u}^{(0)}=-\frac{1}{12\eta(c^{(0)})}(\nabla p^{(0)}-\tilde{G}\rho(c^{(0)})\mathbf{g}), \tag{3.4}$$

and

$$\nabla \cdot \mathbf{u}^{(0)}=-\frac{\rho'}{\rho}(c_t^{(0)}+\mathbf{u}^{(0)}\nabla c^{(0)})=0, \tag{3.5}$$

$$c_t^{(0)}+\mathbf{u}^{(0)}\nabla c^{(0)}=0, \tag{3.6}$$

when $\mathbf{Pe}=1/\gamma$, or

$$\nabla \cdot \mathbf{u}^{(0)}=-\frac{\rho'}{\rho}(c_t^{(0)}+\mathbf{u}^{(0)}\cdot\nabla c^{(0)})$$

$$=\alpha\Delta[f_0'(c^{(0)})+\alpha p^{(-1)}], \tag{3.7}$$

$$\rho(c^{(0)})(c_t^{(0)}+\mathbf{u}^{(0)}\cdot\nabla c^{(0)})=\Delta[f_0'(c^{(0)})+\alpha p^{(-1)}], \tag{3.8}$$

when $\mathbf{Pe}=1$.

Equation (3.3) implies that $p^{(-1)}$ is constant in each outer region. Since $c^{(0)}$ is the constant $c_{1,2}$ in each fluid initially, $c^{(0)}=c_{1,2}$ is the solution to both (3.6) and (3.8). Thus, Eq. (3.5) is satisfied for both choices of $\mathbf{Pe}$. Consequently, at zeroth order in γ, the sharp interface field equations (2.1)–(2.2) are recovered with densities $\rho(c_{1,2})$ and viscosities $\eta(c_{1,2})$. In the BHSCH case, the only change in the above equations is that the α in Eqs. (3.7) and (3.8) should be set to zero which does not alter the conclusion.

2. Inner expansions

To derive the jump conditions (2.3) and (2.4), we perform the matched asymptotic analysis of the HSCH system near the interface. Since the analysis for the BHSCH system is somewhat simpler and yields the same leading order limit as the HSCH system, we do not present that case here.

First we introduce the signed distance function $\psi(x,y,t)$ which measures the distance from the interface; $\psi<0$ denotes the distance to the interface from the fluid 1 direction. The interface is represented by $\Gamma(t)=\{\psi(x,y,t)=0\}$. Next introduce the "stretched" coordinates $\hat{x}$ and $\hat{y}=\psi(x,y,t)/\gamma$, where $\hat{x}$ is taken to be the arc length of the interface. Let $\mathbf{t}$ and $\mathbf{n}$ be the unit vectors in the direction of increasing $\hat{x}$ and $\hat{y}$, respectively. The curvature κ of the interface is $-\Delta\psi$.

In this new coordinate system,

$$\nabla f=\mathbf{t}f_{\hat{x}}+\frac{\mathbf{n}}{\gamma}f_{\hat{y}},$$

$$\Delta f=f_{\hat{x}\hat{x}}+\frac{1}{\gamma^2}f_{\hat{y}\hat{y}}-\frac{\kappa}{\gamma}f_{\hat{y}},$$

$$\nabla \cdot (F_1\mathbf{t}+F_2\mathbf{n})=(F_1)_{\hat{x}}+\frac{1}{\gamma}(F_2)_{\hat{y}}-\kappa F_2.$$

By using hats, we denote the variables in the inner region. We write $\mathbf{u}=\hat{v}\mathbf{t}+\hat{w}\mathbf{n}$ and further suppose that the variables c, v, w, and p have the following expansions in the inner region:

$$\hat{v}(\hat{x},\hat{y},t)=\hat{v}^{(0)}(\hat{x},\hat{y},t)+\gamma\hat{v}^{(1)}(\hat{x},\hat{y},t)+\gamma^2\hat{v}^{(2)}(\hat{x},\hat{y},t)$$
$$+\cdots,$$

$$\hat{w}(\hat{x},\hat{y},t)=\hat{w}^{(0)}(\hat{x},\hat{y},t)+\gamma\hat{w}^{(1)}(\hat{x},\hat{y},t)+\gamma^2\hat{w}^{(2)}(\hat{x},\hat{y},t)$$
$$+\cdots,$$

$$\hat{c}(\hat{x},\hat{y},t)=\hat{c}^{(0)}(\hat{x},\hat{y},t)+\gamma\hat{c}^{(1)}(\hat{x},\hat{y},t)+\gamma^2\hat{c}^{(2)}(\hat{x},\hat{y},t)$$
$$+\cdots,$$

$$\hat{p}(\hat{x},\hat{y},t)=\frac{1}{\gamma}\hat{p}^{(-1)}(\hat{x},\hat{y},t)+\hat{p}^{(0)}(\hat{x},\hat{y},t)+\gamma\hat{p}^{(1)}(x,y,t)$$
$$+\cdots.$$

The matching procedure in the intermediate region where the inner and outer regions overlap is well known (see Ref. 81 for example) and so we do not discuss the details here. At leading order one obtains

$$\hat{c}^{(0)}(\hat{y})\rightarrow c_{1,2}^{(0)}, \tag{3.9}$$

$$\hat{p}^{(0)}(\hat{y})\rightarrow p_{1,2}^{(0)} \tag{3.10}$$
$$\vdots$$

as $\hat{y}\rightarrow\pm\infty$, where the 1, 2 values are the limiting values as the outer variables as (x, y) approach the interface from Ω_1 and Ω_2. Further, let

$$\tilde{\tau}=\tau\Big/\int_{c_2}^{c_1}\rho(c)\sqrt{2(f_0(c)-f_0(c_1)-f_0'(c_1)(c-c_1))}\,dc. \tag{3.11}$$

At $O(1/\gamma^2)$ in the inner expansion of Eq. (2.19), we obtain

$$p^{(-1)}=P(\hat{x})-\rho(\hat{c}^{(0)})(\hat{c}_{\hat{y}}^{(0)})^2. \tag{3.12}$$

By matching with the outer solution and using that $\lim_{\hat{y}\rightarrow\infty}\hat{c}_{\hat{y}}^{(0)}=0$, we find P is independent of $\hat{x}$ and that $p^{(-1)}$ is the same constant P in each region Ω_1 and Ω_2.

Among the $O(1/\gamma)$ equations in the inner expansion of Eqs. (2.18)–(2.21) are the following:

$$\hat{w}_{\hat{y}}^{(0)}=-\frac{1}{\rho(\hat{c}^{(0)})}\rho'(\hat{c}^{(0)})(\psi_t+\hat{w}^{(0)})\hat{c}_{\hat{y}}^{(0)} \tag{3.13}$$

and

$$\hat{p}_{\hat{y}}^{(0)}+(\rho'(\hat{c}^{(0)})\hat{c}^{(1)}(\hat{c}_{\hat{y}}^{(0)})^2+2\rho(\hat{c}^{(0)})\hat{c}_{\hat{y}}^{(0)}\hat{c}_{\hat{y}}^{(1)})_{\hat{y}}$$
$$-\kappa\rho(\hat{c}^{(0)})(\hat{c}_{\hat{y}}^{(0)})^2=0. \tag{3.14}$$

Integrating (3.14) and using the matching conditions, we obtain the jump condition (2.4) for pressure

$$p_2-p_1=\tau\kappa$$

since as we will see presently,

$$\sqrt{2}\int_{c_1}^{c_2}\rho_0(c)\sqrt{f_0(c)-f_0(c_1)-f_0'(c_1)(c-c_1)}\,dc$$
$$=\int_{-\infty}^{+\infty}\rho(\hat{c}^{(0)})(\hat{c}_{\hat{y}}^{(0)})^2\,d\hat{y}. \tag{3.15}$$

Further, integrating (3.13), we get

$$(\psi_t+\hat{w}^{(0)})\rho(\hat{c}^{(0)})=C(t,\hat{x}) \tag{3.16}$$

for some function $C(t,\hat{x})$. We claim that $C(t,\hat{x})=0$ if $\mathbf{Pe}=1/\gamma$ or $\mathbf{Pe}=1$. It will follow from this that

$$w_+=w_-=-\psi_t$$

and hence (2.3) is satisfied.

For the proof of this claim, we let

$$\hat{\mu}=\frac{\partial f_0}{\partial c}-\gamma\frac{\hat{p}}{\rho^2}\frac{\partial\rho}{\partial c}-\frac{\gamma^2}{\rho}\left\{(\rho\hat{c}_{\hat{x}})_{\hat{x}}+\frac{1}{\gamma^2}(\rho\hat{c}_{\hat{y}})_{\hat{y}}-\frac{\kappa}{\gamma}\rho\hat{c}_{\hat{y}}\right\}$$
$$=\hat{\mu}^{(0)}(\hat{x},\hat{y},t)+\gamma\hat{\mu}^{(1)}(\hat{x},\hat{y},t)+\gamma^2\hat{\mu}^{(2)}(\hat{x},\hat{y},t)+\cdots$$

be the inner expansion for the generalized chemical potential.

Case 1: $\mathbf{Pe}=1/\gamma$.

At $O(1/\gamma)$ in the inner expansion of Eq. (2.20), we have

$$\rho(c^{(0)})(\psi_t+\hat{w}^0)\hat{c}_{\hat{y}}^{(0)}=C(t,\hat{x})\hat{c}_{\hat{y}}^{(0)}=\partial_{\hat{y}}^2\hat{\mu}^{(0)}, \tag{3.17}$$

where (3.16) is used. Integrating (3.17) with respect to $\hat{y}$ yields

$$C(t,\hat{x})c^{(0)}=\partial_{\hat{y}}\hat{\mu}^{(0)}+D(t,\hat{x})$$

for some function $D(t,\hat{x})$. Evaluation of this equation at $\hat{y}=\pm\infty$ gives

$$C(t,\hat{x})c_{1,2}=D(t,\hat{x}),$$

which is possible only if $C(t,\hat{x})=D(t,\hat{x})=0$ because $c_1\neq c_2$.

Case 2: $\mathbf{Pe}=1$.

The $O(1/\gamma^2)$ equation in the inner expansion of Eq. (2.20) combined with the matching conditions gives

$$\partial_{\hat{y}}\hat{\mu}^{(0)}=0.$$

Then at $O(1/\gamma)$, the inner expansion in (2.20) reduces to

$$C(t,\hat{x})\hat{c}_{\hat{y}}^{(0)}=\partial_{\hat{y}}^2\hat{\mu}^{(1)}.$$

Thus, the same argument as is used in case 1 implies that $C(t,\hat{x})=0$.

Finally, it remains to show Eq. (3.15) holds. In either the case 1 or case 2, we conclude that

$$\hat{\mu}^{(0)}=a, \tag{3.18}$$

where $a=a(t,\hat{x})$ is a constant in $\hat{y}$. Using a centering condition of the type given in Pego[81] which links Γ with the inner expansion, the argument given in the Appendix of Lowengrub and Truskinovsky[1] shows that $\hat{c}^{(0)}(\hat{y},\hat{x},t)=C_p(\hat{y})$ where $C_p(\hat{y})$ is the planar interface connecting c_1 with c_2 described in Sec. 5 of Ref. 1. From this, one can conclude that Eq. (3.15) indeed is satisfied.

IV. SPECIAL SOLUTIONS

In this section, we consider equilibrium solutions to the HSCH and BHSCH systems. These solutions and their stability, which is analyzed in Sec. V, help to characterize the models. The simplest equilibrium solution for the HSCH and BHSCH models corresponds to a homogeneous solution at rest:

$$c(\mathbf{x},t)=\bar{c}, \quad \mathbf{u}(\mathbf{x},t)=\mathbf{0}, \tag{4.1}$$

where $\bar{c}$ is a constant. Note that there is a balancing linear pressure. More interesting equilibrium solutions are obtained when one considers a stratified binary fluid. That is, the case in which a flat (diffuse) interface separates two infinite regions of nearly pure fluids. Suppose the interface is centered at $y=0$. Then, we may consider the one-dimensional problem in which there is no flow and all variables depend only on y.

A. 1D equilibrium for the BHSCH model

The BHSCH 1D equilibrium equations are

$$q_y=\tilde{G}\tilde{\rho}(c), \tag{4.2}$$

$$\mu_{yy}=0, \tag{4.3}$$

where

$$\mu=f_0'(c)-\mathbf{C}c_{yy}. \tag{4.4}$$

Therefore Eq. (4.3) can be solved independently of Eq. (4.2). An explicit solution may be obtained for at least one choice of $f_0(c)$ with the boundary conditions $c_y=0$ and $c_{yyy}=0$ (from $\mu_y=0$) at $y=\pm\infty$. One can recast these conditions as $\lim_{y\to\pm\infty}c(y)=c_{2,1}$. Let $f_0(c)$ be the quartic function

$$f_0(c)=\frac{\mathbf{D}}{4}(c-c_1)^2(c-c_2)^2, \tag{4.5}$$

which with $D=4$ and $c_1=1$ and $c_2=0$ is the solid curve in Fig. 2. Then, it is easy to see that

$$c(y)=\tfrac{1}{2}[(c_1+c_2)-(c_1-c_2)\tanh((c_1-c_2)y/\sqrt{2\mathbf{C}/\mathbf{D}})]. \tag{4.6}$$

This is known as the Maxwell construction (e.g., Ref. 3) which connects the wells of the free energy f_0 with a common tangent. The modified pressure q is then obtained by integrating Eq. (4.2) in y. Note that this solution is valid whether the fluid is stably or unstably stratified (determined by the sign of $\tilde{G}$). For the more general free energies $f_0(c)$, such as the regular solution model free energy (4.22) considered in the next subsection (dashed curve in Fig. 2), it is not possible to obtain an exact solution and the equilibrium solution is computed numerically. We next discuss how this is done in the context of the HSCH model.

B. 1D equilibrium for the HSCH model

Since the chemical potential μ depends explicitly on q in the HSCH model, it is not possible to find an exact form of the 1D equilibria even for the case of the quartic free energy (4.5) given above. Therefore, numerical simulation is used. To compute the equilibria, we solve the 1D time dependent equations and march in time until equilibria is attained. We took this approach because we encountered difficulty in solving the equilibrium equations directly using a boundary value problem solver. As a consequence, we are able only to obtain the stably stratified equilibria. Although we tried several strategies for computing unstably stratified solutions (including the approach taken in Ref. 86), none were success-

ful. It is not immediately apparent that an unstably stratified 1D equilibrium solution does exist for the HSCH model.

In 1D, the HSCH equations reduce to the following system:

$$v_y=\frac{\alpha}{\mathbf{Pe}}\mu_{yy}, \tag{4.7}$$

$$v=-\frac{1}{12\eta}(q_y-\tilde{G}\rho), \tag{4.8}$$

$$\phi_t+(v\phi)_y=\frac{1}{\mathbf{Pe}}\mu_{yy}, \tag{4.9}$$

where $\rho(c)$ is given by (2.24), the viscosity η is assumed to be constant for simplicity, gravity is in the positive y direction ($\tilde{G}>0$), the chemical potential is

$$\mu=f_0'(c)+\alpha\mathbf{M}q-\mathbf{C}c_{yy},$$

and we have introduced the volume fraction

$$\phi=\rho(c)c. \tag{4.10}$$

Note that as functions of ϕ,

$$\phi(\phi)=\rho_2(1-\alpha\phi), \quad c=\phi/\rho(\phi). \tag{4.11}$$

We suppose (4.7)–(4.9) hold on a sufficiently large finite interval $[-a,a]$ and we impose zero Neumann boundary conditions on c_y and μ_y at the boundaries:

$$c_y=0, \quad \mu_y=0 \quad \text{at} \quad y=\pm a. \tag{4.12}$$

Using these boundary conditions and after some manipulation, Eqs. (4.7)–(4.9) can be recast as a single conservation law for ϕ,

$$\phi_t+f(\phi)_y=0, \tag{4.13}$$

where

$$f(\phi)=v\phi-\frac{1}{\mathbf{Pe}}\mu_y=-\frac{1}{\rho_2\mathbf{Pe}}\rho(c)\mu_y \tag{4.14}$$

is the flux for ϕ, and

$$\mu_y=\frac{\dfrac{1}{12\eta}}{\dfrac{\alpha^2\mathbf{M}}{\mathbf{Pe}}+\dfrac{1}{12\eta}}[(\mu_0(c)-\mathbf{C}c_{yy})_y+\alpha\mathbf{M}\tilde{G}\rho(c)],$$

where $\mu_0(c)\equiv f_0'(c)$ and we actually use (4.11) to replace c in terms of ϕ. This equation is equipped with the boundary conditions

$$\phi_y=0, \quad \mu_y=0 \quad \text{at} \quad y=\pm a. \tag{4.15}$$

Note that the boundary condition on μ implies that

$$c_{yyy}=\frac{\alpha\mathbf{M}}{\mathbf{C}}\tilde{G}\rho(c) \quad \text{at} \quad y=\pm a, \tag{4.16}$$

which directly links gravity with the concentration profile. In the Boussinesq case, $c_{yyy}(\pm a)=0$ since α is taken to be zero in μ.

1. Numerical method for 1D evolution

We use the following conservative finite difference method to solve Eq. (4.13) numerically. We first divide the interval $[-a,a]$ into N cells $I_i=[y_{i-1/2},y_{i+1/2}]$, $1\leq i\leq N$. Let $y_i=\frac{1}{2}(y_{i+1/2}+y_{i-1/2})$ and $\Delta y_i=y_{i+1/2}-y_{i-1/2}$. For simplicity, we assume that these cells have equal lengths and thus that $\Delta y_i=\Delta y$.

Integrating (4.13) over I_i, we obtain the following system:

$$\frac{\partial}{\partial t}\int_{y_{i-1/2}}^{y_{i+1/2}}\phi(y,t)dy+(f(\phi(y_{i+1/2},t))-f(\phi(y_{i-1/2},t)))=0.$$

(4.17)

To achieve second order accuracy, we approximate the solution using the value at cell centers, all derivatives are approximated by second order centered differences, and the integral

$$\int_{y_{i-1/2}}^{y_{i+1/2}}\phi\,dy$$

is approximated by $\Delta y\phi(y_i)$ from the midpoint rule. The resulting semidiscrete equation is

$$\frac{\partial}{\partial t}\phi(y_i,t)+\frac{1}{\Delta y}(f(\phi(y_{i+1/2},t))-f(\phi(y_{i-1/2},t)))=0.$$

(4.18)

Several advantages of this semidiscrete formulation can be easily observed. In view of (4.14), the Neumann boundary conditions (4.15) can be imposed exactly: we simply set $f(\phi_{1/2})=0$, $f(\phi_{N+1/2})=0$ as we evolve (4.18) in the cells I_1 and I_N. Due to this exact numerical implementation of zero Neumann boundary condition for μ and cancellation of fluxes at the cell boundaries in the interior, the mass of ϕ is preserved on the numerical level.

In this semidiscrete system, the primitive variables such as c and ϕ, and their derivatives of even order are computed at the cell centers (primary grid) and their derivatives of odd order are computed at the cell boundaries (dual grid). Whenever we need a value of a variable on one grid computed on the other grid, we take the average of two consecutive values on the other grid. For example, if ρ is needed at $y_{i+1/2}$, it is defined by

$$\rho_{i+1/2}=\tfrac{1}{2}(\rho(c_i)+\rho(c_{i+1})).$$

To advance the solution in time, we use a simple first order forward–backward Euler scheme. Because of the fourth order derivatives in c and the nonlinear relationship between c and ϕ, a little care must be taken to do this. Rather than updating (4.18) directly, we update following coupled system for ϕ and μ:

$$\phi_i^{n+1}=\frac{\Delta t}{\mathbf{Pe}}L_d\mu_i^{n+1}+R_i^n,$$

(4.19)

$$\mu_i^{n+1}=-\frac{\mathbf{C}}{\rho(c_1)}L_d\phi_i^{n+1}+Q_i^n,$$

(4.20)

where

$$R_i^n=\phi_i^n-\frac{\Delta t}{\Delta y}(v_{i+1/2}^n\phi_{i+1/2}^n-v_{i-1/2}^n\phi_{i-1/2}^n)$$

$$+\frac{\alpha\mathbf{M}\Delta t}{\mathbf{Pe}}(q_{yy})_i^n,$$

$$Q_i^n=\mu_0(c_i^n)-\mathbf{CL}_d\left(c_i^n-\frac{1}{\rho(c_1)}\phi_i^n\right).$$

To evaluate $(q_{yy})_i^n$, we take

$$(q_{yy})_i^n=\frac{1}{\Delta y}[(q_y)_{i+1/2}^n-(q_y)_{i-1/2}^n],$$

$$\left(\frac{\alpha^2\mathbf{M}}{\mathbf{Pe}}+\frac{1}{12\eta}\right)(q_y)_{i+1/2}^n=-\frac{\alpha}{\mathbf{Pe}}(\mu_0(c)_y)_{i+1/2}^n$$

$$+\frac{G}{12\eta}\rho(c_{i+1/2}^n),$$

in the interior of the dual grid. At the boundary, we take $q_y=G\rho(c)$. To calculate $(\mu_0(c)_y)_{i+1/2}^n$, we use

$$(\mu_0(c)_y)_{i+1/2}^n=\frac{1}{\Delta y}[\mu_0(c_{i+1}^n)-\mu_0(c_i^n)].$$

Note that by the definition of ϕ,

$$c-\frac{1}{\rho(c_1)}\phi\approx0$$

(4.21)

away from the transition region since $c_1\approx1$ and $c_2\approx0$. We will also take advantage of this fact when we solve the full equations in paper II.[2] Finally, L_d is the discrete Laplacian in 1D associated with the zero Neumann boundary condition, that is,

$$L_df_i=\begin{cases}\dfrac{1}{(\Delta y)^2}(f_{i+1}-2f_i)+f_{i-1} & \text{for } 1<i<N,\\[2mm]\dfrac{1}{(\Delta y)^2}(f_{i+1}-f_i) & \text{for } i=1,\\[2mm]\dfrac{1}{(\Delta y)^2}(-f_i+f_{i-1}) & \text{for } i=N.\end{cases}$$

An advantage of our fully discrete formulation is that the resulting linear system for ϕ^{n+1} and μ^{n+1} can be solved directly using a block tridiagonal solver.

2. Numerical results for 1D evolution

We first solved Eqs. (4.19)–(4.20) using the quartic free energy f_0 given in Eq. (4.5) with $c_1=1$ and $c_2=0$ and $\rho_2=1$ and $\rho_1=0.9091$. Interestingly the code diverges for the following reason. Both antidiffusion and gravity drive the separation of light and heavy fluid, although the chemical diffusion "turns off" when $c\approx c_1$, c_2 since $\Delta\mu_0(c_{1,2})=0$. Gravity, however, continues to drive the separation even when $c\approx c_1$, c_2 (e.g., recall the boundary condition for c_{yyy}) and the fluids "pile up" at the boundaries. As this occurs, the concentration becomes negative near the fluid 2 boundary since there is no maximum principle for the concentration equation with the quartic free energy and constant mobility;

recall that Eq. (4.13) is a fourth order nonlinear diffusion equation. The negative concentration eventually causes the density $\rho(c)$ to diverge.

To overcome this difficulty, we use the regular solution model free energy

$$f_0(c) = A[c \ln c + (1-c)\ln(1-c)] - \frac{B}{2}[c^2 + (1-c)^2] + E,$$
(4.22)

which is singular at $c = 0, 1$ and hence constrains $c(y,t)$ to remain between 0 and 1 for all t (e.g., see Ref. 87). The constants c_1 and c_2 are then determined as the minima of $f_0(c)$. When we set $A = 0.5$, $B = 1.5$, and $E = 0.7841$ we can see in Fig. 2 that this regular solution free energy (dashed curve) compares well with the quartic free energy (solid curve). For the above choice of A and B, we have

$$c_1 = 0.9293, \quad c_2 = 0.0707,$$

which are found using Newton's method. For the density, we prescribe the equilibrium densities $\rho(c_1) = 1/(1+\beta)$ and $\rho(c_2) = 1$ instead of ρ_1 and ρ_2 which are the densities before mixing. The connection between the two is given by

$$\alpha = \frac{1}{\rho_1} - \frac{1}{\rho_2} = \beta/(c_1 - c_2),$$
(4.23)

$$\frac{1}{\rho_2} = \beta + 1 - \frac{c_1 \beta}{c_1 - c_2}.$$
(4.24)

Note that when $c_1 = 1$ and $c_2 = 0$, the two density descriptions are identical. In addition, β is a non-negative constant that is varied. Thus, fluid 1 is the lighter fluid of the two.

We define $\mathbf{C}$ and $\mathbf{M}$ by the scaling (3.2) and we set $\mathbf{Pe} = 1/\gamma$. In the simulations presented below, we take $\gamma = 0.1$. The surface tension is $\tau = \sqrt{2}/6$, the viscosity is $\eta = 0.5$ and the gravitational constant $\tilde{G}$ is determined from the Bond number as follows:

$$\tilde{G} = \frac{B}{\tau}(\rho(c_2) - \rho(c_1)),$$
(4.25)

with $\mathbf{B} = 25$. Note that the Atwood number $\mathbf{A} = 0$. In the remainder of the paper, this value of τ is fixed and so changing $\mathbf{B}$ is equivalent to changing $\tilde{G}$ via Eq. (4.25).

Last, the numerical parameters are given as follows. We consider the domain $-2.5 \leq y \leq 2.5$ and use $N = 1000$ grid points. We use the time step $\Delta t = 5.0 \times 10^{-4}$ initially and we refine the time step if $c(\pm 2.5, t)$ approaches 0 or 1, the singular points of the logarithmic $f_0(c)$. More precisely, if $|c(\pm 2.5, t) - c_{\text{sing}}| < d$ where $c_{\text{sing}} = 0, 1$ then $\Delta t = \epsilon_{\Delta t} \Delta t_{\text{old}}$ and $d = \epsilon_d d_{\text{old}}$ where $d_{\text{initial}} = 2.5 \times 10^{-3}$, $\epsilon_{\Delta t} = 0.5$ and $\epsilon_d = 0.8$.

The equilibrium solutions for $\beta = 0$ and $\beta = 0.1$ (the stably stratified case) are shown in Fig. 3. In the upper graph, c is shown while in the lower graphs the numerical flux and its components are shown. Note that when $\beta = 0$, the concentration and pressure equations decouple at equilibrium and the resulting concentration solution c is the equilibrium for the Boussinesq model. The $\beta = 0$ solution (dashed curve) smoothly connects c_1 and c_2 and resembles the hyperbolic

tangent (4.6) as the profile approaches the boundary with zero slope. Since f_0 is the regular solution free energy, the $\beta = 0$ solution is different from Eq. (4.6) though.

The presence of the pressure in the chemical potential when $\beta = 0.1$, on the other hand, causes a surprising difference between the two cases away from the transition layer. In the $\beta = 0.1$ case (solid curve), gravity additionally drives the density stratification and causes the fluids to be more "pure" away from the transition layer; that is, c is closer to 0 and 1. This seems quite reasonable physically. At the boundaries, for example, $c(-2.5) = 0.9971$ and $c(2.5) = 0.0023$. In addition, the profile does not approach the boundary with zero slope because of the boundary condition on c_{yyy}. We have tried other values of β and found similar behavior. Moreover, we have also considered the effect of domain size. Increasing the size of the domain causes the limiting concentrations to be closer to 0 and 1 but does not change the transition profile significantly. This suggests that in the limit of an infinite domain (with $\beta > 0$), the values of c at $y = \pm \infty$ are 0 and 1 [the singular values of $f_0(c)$] rather than c_1 and c_2 [the minima of $f_0(c)$] as is the case in the BHSCH model.

By considering the numerical flux, we can understand how such a profile can be in equilibrium. Consider Fig. 3(b). In this plot, all the components of the flux $f(\phi)$ are shown. The total flux is indicated by "o" and is seen to be zero. The pressure contribution (q) to the flux is nearly constant (dotted–dashed curve) and has only a small variation across the transition layer due to the small density variation (since $\beta = 0.1$). Near the transition layer, the μ_0 (solid curve) and c_{yyy} (dashed curve) contributions dominate and balance one another. At the boundaries [shown in Fig. 3(c)], a boundary layer is seen in the μ_0 and c_{yyy} terms and it is the latter that balances the pressure at the boundary. Note that in the interior of the domain (e.g., $-2.4 \leq y \leq -0.5$), the flux from c_{yyy} is nearly zero.

To examine the evolution process, we consider the approach to steady state of an initially unstably stratified binary fluid. This is shown in plot of Fig. 4(a). The initial state (solid curve) is a hyperbolic tangent connecting c_2 at $y = -2.5$ with c_1 at $y = 2.5$. All parameters are as in the previous simulation; this makes the stratification unstable. Observe that fluid is fluxed through the domain and that the light and heavy fluids pile up at $y = -2.5$ and $y = 2.5$, respectively. The light/heavy interfaces move in from the boundaries and eventually meet at the center of the domain as the profile equilibrates. The flux $f(\phi)$ is shown in Figs. 4(b) and 4(c) at time $T = 1.5$ and the behavior is analogous to that seen in Fig. 3 except that now there are more transition layers.

Finally, let us interpret our equilibrium results in view of the sharp interface asymptotics presented in Sec. III. In that section, it was seen that the same sharp interface limit is obtained at leading order for both the HSCH and BHSCH models. In the 1D case this means that across $y = 0$, c should jump from c_1 to c_2. Now, although the equilibrium profiles of c for $\beta = 0$ and $\beta = 0.1$ appear to be quite different away from the transition layer, they actually only differ by an $O(\gamma)$ amount since $\gamma = 0.1$. Further, when γ is reduced to $\gamma = 0.05$, two things happen. The width of the transition layer
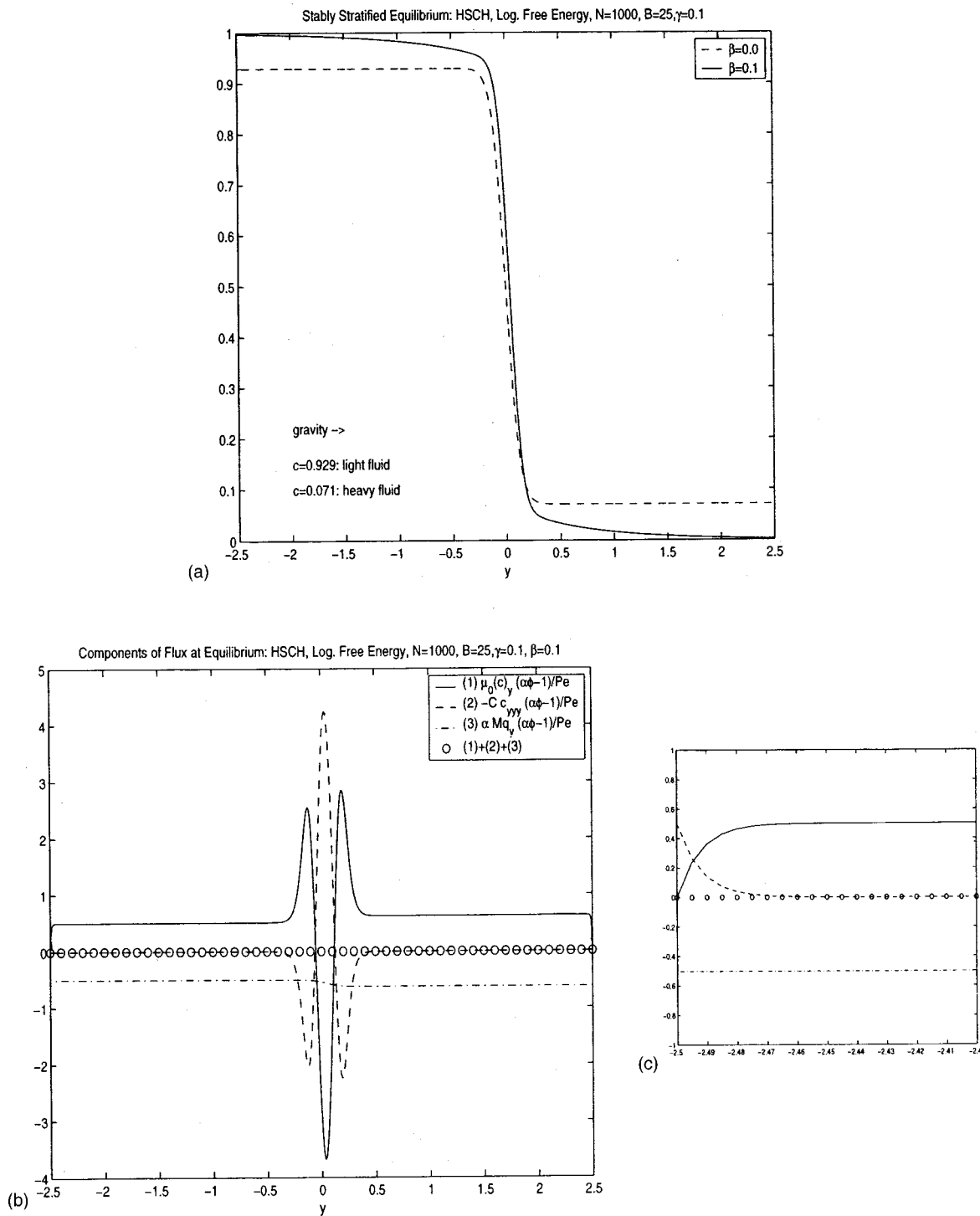
FIG. 3. Stably stratified equilibrium, $B=25$ and $\gamma=0.1$. (a) Concentration, $\beta=0$ (dashed curve), $\beta=0.1$ (solid curve); (b) components of the flux. Total flux ($\bigcirc$ curve), $\mu_0(c)_y(\alpha\phi-1)/\mathbf{Pe}$ (solid curve), $-\mathbf{C}c_{yyy}(\alpha\phi-1)/\mathbf{Pe}$ (dashed curve), $\alpha\mathbf{M}q_y(\alpha\phi-1)/\mathbf{Pe}$ (dotted–dashed curve); (c) close-up of the components near the boundary point $y=-2.5$.

decreases by a factor of 2 (as expected) and the values of c at the boundary become closer to c_1 and c_2 [i.e., $c(-2.5)=0.9872$ and $c(2.5)=0.01131$] albeit at a slow rate. This is consistent with the sharp interface asymptotics and we interpret the slow rate of approach as follows. We believe that the effect of gravity on the chemical potential (through the pressure) is magnified by both the geometry (1D single transition

layer) and equilibrium nature of the problem. For example, as may be seen in paper II,[2] dynamical simulations of the full HSCH and BHSCH models, in periodic domains with two transition layers, yield very similar results for comparable values of γ away from pinchoff and reconnection. This is likely due to the fact that because of the periodic boundary conditions, there are no boundary layers in the HSCH case.
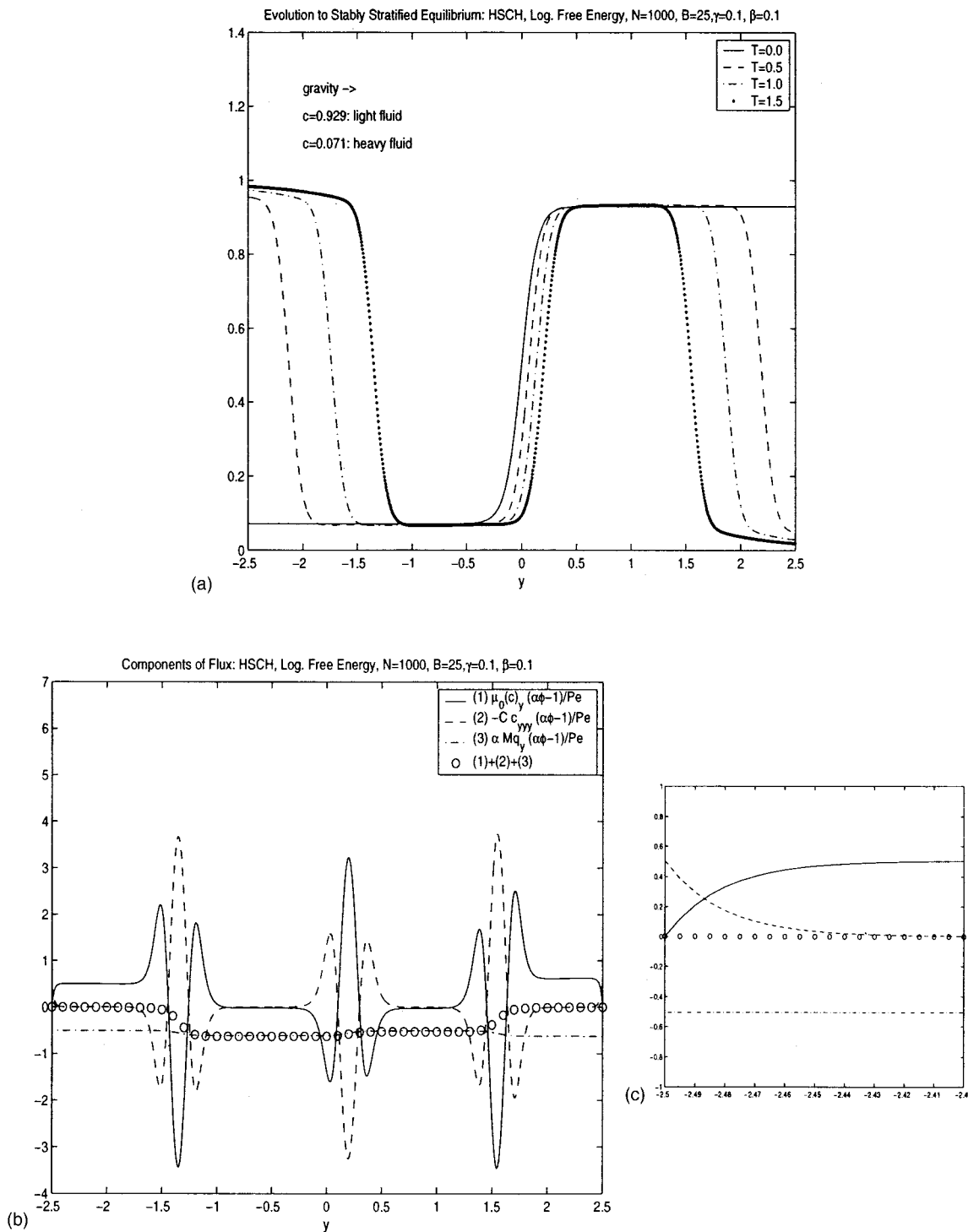
FIG. 4. Evolution to the stably stratified equilibrium. $B = 25$, $\gamma = 0.1$, and $\gamma = 0.1$. (a) Concentration at times $t = 0$ (solid curve), $t = 0.5$ (dashed curve), $t = 1.0$ (dotted–dashed curve) and $t = 1.5$ (dotted curve); (b) components of the flux at $t = 1.5$ marked as in Fig. 3; (c) close up of the components near the boundary point $y = -2.5$.

V. LINEAR STABILITY ANALYSIS

In this section, we consider the linear stability of the equilibrium solutions we obtained in the preceding section. We focus primarily on the two cases for which we have exact formulas for the equilibrium solution (1) the stability of homogeneous solutions at rest for the HSCH and BHSCH models and (2) the stability of the unstably stratified 1D equilib-rium solution to two-dimensional perturbations in the BHSCH model. Since we do not have an analytical or numerical representation of an unstably stratified 1D equilibrium solution for the HSCH model, we make a practical comparison between the growth rates for the two models, at the end of this section, by solving the full equations numerically in the linear regime.

A. Linear stability of homogeneous solutions

Let us consider solutions to the HSCH Eqs. (2.18)–(2.21) of the form

$$c(\mathbf{x},t) = \bar{c} + \epsilon\tilde{c}(\mathbf{x},t), \tag{5.1}$$

$$\mathbf{u}(\mathbf{x},t) = \mathbf{0} + \epsilon\tilde{\mathbf{u}}(\mathbf{x},t), \tag{5.2}$$

$$q(\mathbf{x},t) = \bar{q} + \epsilon\tilde{q}(\mathbf{x},t), \tag{5.3}$$

$$\mu(\mathbf{x},t) = \bar{\mu} + \epsilon\tilde{\mu}(\mathbf{x},t), \tag{5.4}$$

where $\bar{c}$ is a constant, $\bar{q} = \tilde{G}\rho(\bar{c})y$ and $\bar{\mu} = \mu_0(\bar{c}) + \alpha\mathbf{M}\tilde{G}\rho(\bar{c})y$ are the equilibrium values of concentration, pressure, and chemical potential, respectively. Gravity is assumed to be in the y direction. Plugging Eqs. (5.1)–(5.4) into the HSCH system, keeping terms proportional to ϵ and rewriting the resulting linear system as a single equation for $\tilde{c}$, we obtain the advection–diffusion equation

$$\tilde{c}_t + v_l\tilde{c}_y = D_l\Delta[f_0''(\bar{c})\tilde{c} - \mathbf{C}\Delta\tilde{c}], \tag{5.5}$$

where the advection velocity v_l is given by

$$v_l = \rho(\bar{c})\frac{\alpha^2\mathbf{M}\eta(\bar{c})}{\mathbf{Pe} + 12\alpha^2\mathbf{M}\eta(\bar{c})}\tilde{G}, \tag{5.6}$$

and we have used the simple mixture formula (2.24) for the density. The diffusion coefficient D_l is given by

$$D_l = \frac{1}{\rho(\bar{c})[\mathbf{Pe} + 12\alpha^2\mathbf{M}\eta(\bar{c})]}. \tag{5.7}$$

The advection velocity arises from the dependence of the chemical potential on the pressure. Observe that as a consequence, there is flow in the direction of gravity. This makes sense physically and is consistent with the 1D evolution we investigated in the previous section for the HSCH model. Using the scaling (3.2) the advection velocity is $O(\alpha^2\gamma^2\tilde{G})$ which vanishes as the interface thickness $\gamma \to 0$.

Looking for a solution of Eq. (5.5) in the form of a normal mode $\tilde{c} = e^{i\mathbf{k}\cdot\mathbf{x} + \sigma t}$, we obtain the following dispersion relation between the wave number $\mathbf{k} = (k_1, k_2)$ and the growth rate σ:

$$\sigma = -v_l ik_2 + \mathbf{C}D_l|\mathbf{k}|^2(k_C^2 - |\mathbf{k}|^2), \tag{5.8}$$

where k_C is the critical wave number

$$k_C^2 = -f_0''(\bar{c})/\mathbf{C}, \tag{5.9}$$

which was first identified in the context of the spinodal decomposition for binary alloys (e.g., see Ref. 88). From Eqs. (5.8) and (5.9), we see that growth may occur for those wave numbers $\mathbf{k}$ such that $|\mathbf{k}| < k_C$ if $f_0''(\bar{c}) < 0$. Otherwise, the solutions decay.

The linearized equation for $\tilde{c}$ in the BHSCH model is obtained by simply setting $\alpha = 0$ and $\rho(\bar{c}) = 1$ in Eqs. (5.5)–(5.7). This gives

$$\tilde{c}_t = \frac{1}{\mathbf{Pe}}\Delta[f_0''(\bar{c})\tilde{c} - \mathbf{C}\Delta\tilde{c}]. \tag{5.10}$$

Note that there is no flow. Equation (5.10) is identical to the classical Cahn–Hilliard equation[46] linearized about a constant state (again see Ref. 88). The growth rate of a normal mode is

$$\sigma = \frac{1}{\mathbf{Pe}}|\mathbf{k}|^2(k_C^2 - |\mathbf{k}|^2), \tag{5.11}$$

and thus the condition for growth or decay of modes is the same as that in the HSCH model.

B. Linear stability of the 1D BHSCH equilibrium solution

We now consider the linear stability of the unstably stratified 1D equilibrium solution of the BHSCH model to two-dimensional perturbations. In this section, we present equations governing the linear growth rates of the perturbations. We solve these equations numerically and compare the resulting growth rates to those from the sharp interface model given in Sec. II A. We demonstrate the linear convergence of the two growth rates as the interface thickness is taken to zero (following the scaling in Sec. III). Through this comparison, we study the effect of the **Pe**, **C**, and **M** numbers on the linear growth rates. We then use this knowledge later in our numerical simulations of the full equations.

We focus on the unstably stratified case because there is the potential for perturbations to grow, in contrast to the decay found in the stably stratified case. Thus, the stabilizing effects of the chemical diffusion and interface thickness are easy to identify. For simplicity, we suppose that the viscosity η is constant.

Let us consider the solution to Eqs. (4.2)–(4.4) with the quartic free energy $f_0(c)$ given in (4.5) with $\mathbf{D} = 4$, $c_1 = 1$, and $c_2 = 0$. For the density, we take

$$\tilde{\rho}(c) = 1 - \alpha_g c, \tag{5.12}$$

where α_g is a positive constant. Therefore $1 = \tilde{\rho}(0) > \tilde{\rho}(1) = 1 - \alpha_g$. The unstably stratified equilibrium solution is then either given by Eq. (4.6) with $\tilde{G} < 0$ (gravity pointing in negative y direction) or by reversing the roles of c_1 and c_2 in (4.6) and keeping $\tilde{G} > 0$. In the results we present below, we take the former approach.

Next we consider the following perturbations of the 1D BHSCH equilibrium:

$$\mathbf{u}(x,y,t) = \mathbf{0} + \epsilon\hat{\mathbf{u}}(y)e^{ikx + \sigma t},$$

$$c(x,y,t) = \bar{c}(y) + \epsilon\hat{c}(y)e^{ikx + \sigma t},$$

$$q(x,y,t) = \bar{q}(y) + \epsilon\hat{q}(y)e^{ikx + \sigma t},$$

where $\bar{c}(y)$ is given in Eq. (4.6) and $\bar{q}(y)$ is obtained by using $\bar{c}(y)$ in Eq. (4.2).

The linearized equations for the perturbations are

$$ik\hat{u} + \hat{v}_y = 0, \tag{5.13}$$

$$-12\eta\hat{u} = ik\left(\hat{q} + \frac{\mathbf{C}}{\mathbf{M}}(\bar{c}_{yy}\hat{c} - \bar{c}_y\hat{c}_y)\right), \tag{5.14}$$

$$-12\eta\hat{v} = \hat{q}_y - k^2\frac{\mathbf{C}}{\mathbf{M}}\bar{c}_y\hat{c} + \tilde{G}\rho'(\bar{c})\hat{c}, \tag{5.15}$$

$$\sigma\hat{c}+\bar{c}_y\hat{v}=\frac{1}{\mathbf{Pe}}\left(\frac{d^2}{dy^2}-k^2\right)\left(\mu_0'(\bar{c})\hat{c}-\mathbf{C}\left(\frac{d^2}{dy^2}-k^2\right)\hat{c}\right). \tag{5.16}$$

Equations (5.13)–(5.16) can be reduced to a coupled system consisting of a second order equation for $\hat{q}$ and a fourth order equation for $\hat{c}$ as follows:

$$\hat{q}_{yy}=k^2\hat{q}+2k^2\frac{\mathbf{C}}{\mathbf{M}}\bar{c}_{yy}\hat{c}+\alpha_g\widetilde{G}\hat{c}_y \tag{5.17}$$

and

$$\hat{c}_{yyyy}=\frac{\mathbf{Pe}}{12\eta\mathbf{C}}\bar{c}_y\hat{q}_y+\frac{2}{\mathbf{C}}\mu_0''(\bar{c})\bar{c}_y\hat{c}_y+\left(\frac{1}{\mathbf{C}}\mu_0'(\bar{c})+2k^2\right)\hat{c}_{yy}$$

$$+\left[-k^4+\frac{1}{\mathbf{C}}(\mu_0'''(\bar{c})\bar{c}_y^2+\mu_0''(\bar{c})\bar{c}_{yy}-k^2\mu_0'(\bar{c}))\right.$$

$$\left.-\sigma\frac{\mathbf{Pe}}{\mathbf{C}}-\frac{\mathbf{Pe}}{12\eta\mathbf{C}}\bar{c}_y\left(k^2\frac{\mathbf{C}}{\mathbf{M}}\bar{c}_y+\alpha_g\widetilde{G}\right)\right]\hat{c}. \tag{5.18}$$

The boundary conditions for these equations are

$$\hat{q}\to0,\quad\hat{c}\to0\quad\text{as }y\to\pm\infty. \tag{5.19}$$

Next, observe from Eq. (4.6) that $\bar{c}(y)-\frac{1}{2}$ is an odd function of y, and thus

$$\mu_0'(\bar{c})=\frac{\mathbf{D}}{2}[4(\bar{c}-\tfrac{1}{2})^2+2((\bar{c}-\tfrac{1}{2})^2-\tfrac{1}{4})]$$

even,

$$\mu_0''(\bar{c})=3\mathbf{D}(2\bar{c}-1)$$

is odd, and

$$\mu_0'''(\bar{c})=6\mathbf{D}$$

is even. These facts lead us to expect symmetric solutions (odd $\hat{q}$ and even $\hat{c}$) to Eqs. (5.17) and (5.18). Our numerical method will take advantage of this symmetry and we solve Eqs. (5.17) and (5.18) on only half of the domain.

Before concluding this section, we present the sharp interface growth rate for this flow for purposes of comparison:

$$\sigma_0=-\frac{\tau}{24\eta}(|k|^3+\mathbf{B}|k|), \tag{5.20}$$

where τ is the surface tension and $\mathbf{B}$ is the bond number (2.5). Therefore, when $\mathbf{B}<0$ there is a range of unstable modes near $k=0$ due to unstable density stratification.

Although we do not present it here, we have performed matched asymptotic expansions for Eqs. (5.17) and (5.18) for the scaling and general procedure outlined in Sec. III. We obtained the sharp interface growth rate σ_0 at leading order, but we were unable to calculate the next order correction in closed form. Consequently, we solve the full Eqs. (5.17) and (5.18) numerically to compare σ with σ_0.

1. Numerical methods for linear growth rates

We solve Eqs. (5.17)–(5.19) on a large, but finite interval $[-a,a]$. The transition region is centered around $y=0$ and our matched asymptotic expansions suggest that the solutions decay exponentially fast in $|y|$ away from this layer.

This is confirmed by numerical experiments and the computed linear growth rates are insensitive to the size of the interval $[-a,a]$ as long as $a\gg\sqrt{\mathbf{C}}$.

To take advantage of the symmetry of the solutions, we solve Eqs. (5.17)–(5.19) on the half interval $[0,a]$ and we prescribe the following boundary conditions at $y=0$:

$$\hat{q}=0,\quad\hat{c}_y=0,\quad\hat{c}_{yyy}=0,\quad\hat{c}=b,\quad\text{at }y=0, \tag{5.21}$$

where b is a numerical parameter which is discussed below. At $y=a$, we pose

$$k\hat{q}(a)+\hat{q}_y(a)=0,\quad\hat{c}_{yy}(a)=0, \tag{5.22}$$

where the first term in (5.22) is suggested by the outer leading order equations in the matched asymptotic expansions of Eqs. (5.17)–(5.19). We account for the exponential decay in $\hat{q}$ and not $\hat{c}$ because the rate of decay of $\hat{q}$ depends on the wave number k. Hence $\hat{q}$ decays slowly for small k. In contrast, the rate of decay of $\hat{c}$ is independent of k.

Although there are six boundary conditions in total, the condition $\hat{c}_{yy}(a)=0$ does not imply that $\hat{c}(a)=0$. Consequently, solutions can be found for all values of σ with boundary conditions (5.21) and (5.22) but there is only one value of σ for which $\hat{c}(a)=0$ in addition. Note that if the domain is large enough, $\hat{c}(a)=0$ implies $\hat{c}_{yy}(a)\approx0$ with the $\approx$ becoming $=$ in the infinite domain limit.

Following Ref. 89, we use a version of Keller's method[90] in which the growth rate is determined as the value of σ which produces the correct boundary value $\hat{c}=0$ at $y=a$. Let $\hat{c}(y,k,\sigma)$ represent the solution of Eqs. (5.17)–(5.19) for a given k and σ. For each k, starting with an initial guess for $\sigma_{k,0}$, we generate a sequence $\{\sigma_{k,i}\}$ converging to the root of

$$\hat{c}(a,k,\sigma_k)=0$$

using an iterative root finding method. To compute $\hat{c}(a,k,\sigma_{k,i})$ for each $\sigma_{k,i}$, we solve the boundary value problem (5.17)–(5.19) using the FORTRAN routine COLNEW and we use Brent's method to find the root. Both routines are available from NETLIB. The numerical constant b in (5.21) is set to a nonzero number in order to obtain a nontrivial solution $\hat{c}$.

2. Numerical linear growth rates

We take $a=2.5$, $b=10^{-3}$ and use 800 grid points in solving the boundary value problem (5.17)–(5.19). For $\mathbf{C}$, $\mathbf{M}$, and $\mathbf{Pe}$ numbers, we take the values given in (3.2) with $\gamma=0.05$. The viscosity is $\eta=1/2$, the surface tension is $\tau=\sqrt{2}/6$ and gravity $\widetilde{G}$ is determined from the Bond number $\mathbf{B}=-25$ and $\alpha_g=0.091$ via Eqs. (5.12) and (4.25).

We begin by considering the effect of $\mathbf{Pe}$. In Fig. 5(a), the linear growth rates are shown for the sharp interface model [solid curve; σ_0 from Eq. (5.20)], the BHSCH model with $\mathbf{Pe}=1/\gamma$ ($\bigcirc$) and with $\mathbf{Pe}=1$ (+). The growth rates from the BHSCH model with $\mathbf{Pe}=1/\gamma$ are much closer to σ_0 than are the growth rates with $\mathbf{Pe}=1$. Decreasing the $\mathbf{Pe}$ number increases dissipation and decreases the linear growth rate. So, even though our asymptotic analysis in Sec. III indicates that both scalings of $\mathbf{Pe}$ yield the classical sharp
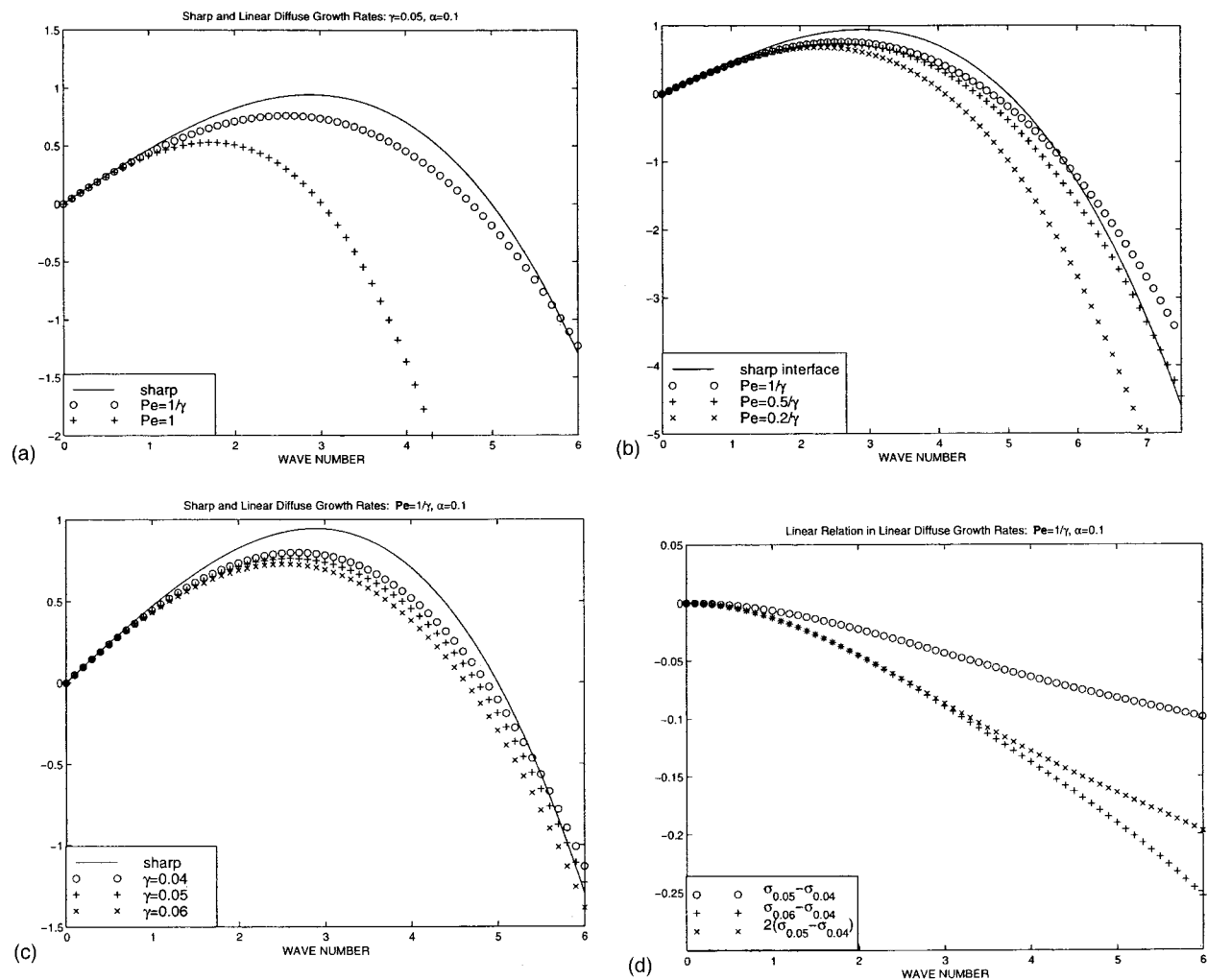
FIG. 5. Sharp and diffuse interface growth rates in Boussinesq approximation. $B = -25$, $\alpha = 0.1$ (a). Sharp interface (solid curve), BHSCH with $\mathbf{Pe} = 1/\gamma$ ($\bigcirc$ curve), BHSCH with $\mathbf{Pe} = 1$ (+ curve). In BHSCH, $\gamma = 0.05$. (b) Sharp interface (solid curve), BHSCH with $\mathbf{Pe} = 1/\gamma$ ($\bigcirc$ curve), BHSCH with $\mathbf{Pe} = 0.5/\gamma$ (+ curve), BHSCH with $\mathbf{Pe} = 0.2/\gamma$ ($\times$ curve). Again, $\gamma = 0.05$. (c) Sharp interface (solid curve). BHSCH with $\mathbf{Pe} = 1/\gamma$, $\gamma = 0.04$ ($\bigcirc$ curve), $\gamma = 0.05$: + curve, $\gamma = 0.06$ ($\times$ curve). (d) Difference between sharp and BHSCH growth rates. $\sigma_{0.05} - \sigma_{0.04}$ ($\bigcirc$ curve), $\sigma_{0.06} - \sigma_{0.04}$ (+ curve), $2(\sigma_{0.05} - \sigma_{0.04})$ ($\times$ curve).

interface model at leading order as $\gamma \to 0$, this graph suggests that for a fixed value of γ, the $\mathbf{Pe} = 1/\gamma$ scaling yields a closer approximation to the sharp interface. Consequently, we use this scaling in our simulations of the full BHSCH and HSCH models presented in paper II.[2]

Figure 5(a) also indicates that the $\mathbf{Pe} = 1/\gamma$ growth rates become less negative than σ_0 for wave numbers $k > 5.8$ suggesting that the BHSCH model is less dissipative than the sharp interface model at those wave numbers. In a simulation of the full equations with initial data containing linearly unstable modes, it is difficult to observe the lowered dissipation since growth dominates. Nevertheless, one can modify the $\mathbf{Pe}$, still keeping $\mathbf{Pe} = O(1/\gamma)$, so as to increase damping at high wave numbers. This is shown in Fig. 5(b) where σ_0 (solid curve) and the growth rates with $\mathbf{Pe} = 1/\gamma$ ($\bigcirc$) $\mathbf{Pe} = 0.5/\gamma$ (+), $\mathbf{Pe} = 0.2/\gamma$ ($\times$) are shown. Not surprisingly, observe that decreasing $\mathbf{Pe}$ tends to affect the behavior at high wave numbers much more than at low wave numbers. Interestingly, the diffuse interface model of Folch et al.[83] seems to produce a qualitatively similar dispersion relation as shown here for the BHSCH model with $\mathbf{Pe} = 1/\gamma$. We find

this a little surprising given that our model equations seem quite different.

Next, we consider the effect of γ on the linear growth rates. In Fig. 5(c), we take $\mathbf{Pe} = 1/\gamma$ and consider the growth rates when $\gamma = 0.06$ ($\times$), 0.05 (+), and 0.04 ($\bigcirc$). For comparison, σ_0 is also shown (solid curve). The growth rates are seen to be increasing functions of γ and approach the σ_0 curve. To measure the rate of approach, consider the differences between the different growth rates at different values of γ. This is shown in Fig. 5(d). Observe that the convergence is linear in γ at small wave numbers. This is consistent with the matched asymptotics presented in Sec. III. Decreasing γ further leads to a larger region of linear convergence.

Finally, we comment on the effect of other parameters on the BHSCH growth rates. Letting $\mathbf{C} = \gamma^2$, this parameter measures the closeness of the sharp and BHSCH growth rates. Letting $M = M_0 \gamma$, the parameter M_0 can be used to adjust both the wave number k_m and magnitude of the maximum growing mode by effectively modifying the surface tension. The initial slope, near $k = 0$, can be altered by changing $\mathbf{B}$ (i.e., gravity). Since our asymptotic analysis and nu-

merical results predict linear convergence of the BHSCH and sharp interface growth rates, we can modify M_0 from Eq. (3.2) and $\mathbf{B}$ by an $O(\gamma)$ amount and still achieve the same leading order sharp interface growth rate. We can take advantage of this fact as follows.

By modifying M_0, $\mathbf{B}$, and $\mathbf{Pe}$ by an $O(\gamma)$ amount to better match the growth rates of the BHSCH and sharp interface models at finite values of γ, we may achieve better agreement between the solutions of the fully nonlinear systems. This idea is quite general and, in spirit, is analogous to the improvements in a phase field model for solidification, suggested by Karma and Rappel,[91] in which the phase-field equations are modified to remove first order effects of interface kinetics in the sharp interface limit. In our case, we can try to match the growth rates of all the unstable wave numbers or we can try to match only the growth rate of the most unstable wave number or perhaps just the most unstable wave number present in an initial condition.

We have investigated all of these approaches and found that while they all yield better approximations of the sharp interface model (measured from simulations of the full BHSCH/HSCH equations) than the original values of M_0, $\mathbf{B}$, and $\mathbf{Pe}$, the best agreement between the BHSCH (and HSCH) and sharp interface models is achieved when the growth rate of the most unstable wave number in an initial condition is matched. On the one hand, this is a little unsatisfactory because this suggests that the appropriate BHSCH (and HSCH) parameters are initial data dependent. On the other hand, the parameters may be precalculated without reference to the specific initial condition; the parameters only depend on which wave numbers are present, the interface thickness and the physical constants governing the flow. We are unable to explain fully why matching more than the most unstable wave number in an initial condition does not yield a better result. Perhaps the answer lies in the fact that our attempts to match the growth rates of a band of unstable modes are only approximate and in that band no growth rates are matched exactly—they are all uniformly approximated. With a single wave number, however, we can exactly match the growth rate. Thus, it may be that the choices of M_0, $\mathbf{B}$, and $\mathbf{Pe}$, we used in our attempt to match the band of unstable modes, were not optimal.

In paper II,[2] we present several simulations of the fully *nonlinear* BHSCH and HSCH models with different initial data in which the growth rates at wave numbers 1 and 3 are matched to σ_0, respectively, with each corresponding to the most unstable wave number in the initial condition. In preparation for these simulations, we indicate how matching the growth rates at $k=1$ and $k=3$ may be achieved by modifying only $\mathbf{B}$. Let $\mathbf{B} = -25(1+b\gamma)$, $\mathbf{Pe} = 1/\gamma$ and all other parameters as before. From Fig. 6(a), we conclude that the BHSCH growth rates depend linearly on b. We then use linear interpolation to determine the values of $b=b_{k,\gamma}$ required to match the growth rates for a given wave number k and interface thickness γ. This is shown in Fig. 6(b) for $k=1$ and $\gamma = 0.05$, 0.04. We obtain $b_{1,.05} = 1.4148$ and $b_{1,.04} = 1.4025$. Analogously, we obtain $b_{3,.05} = 3.3782$ and $b_{3,.04} = 3.2101$ at wave number $k=3$. Observe that $b_{k,\gamma}$ is a decreasing function of γ for these two wave numbers.
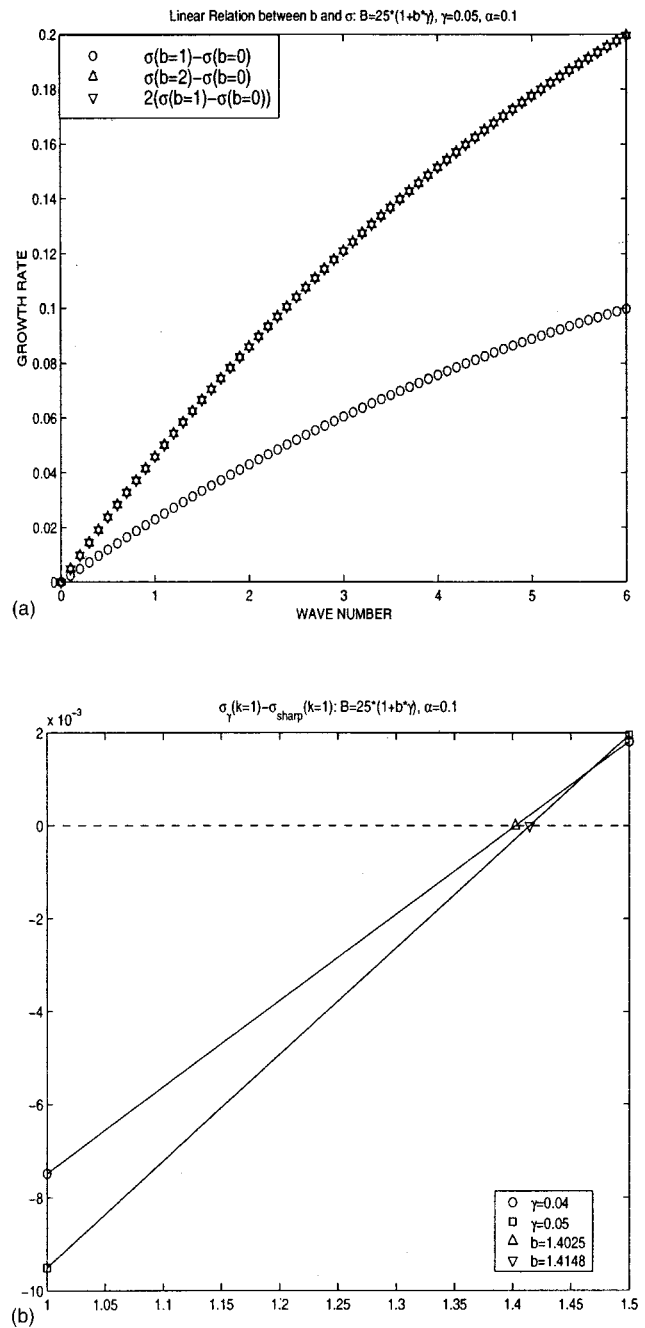

FIG. 6. (a) Linear relation between b and the growth rates with $\gamma = 0.05$ and $\mathbf{B} = -25*(1+b\gamma)$. $\sigma(b=1)-\sigma(b=0)$ ($\bigcirc$ curve), $\sigma(b=2)-\sigma(b=1)$ (triangle curve), $2(\sigma(b=1)-\sigma(b=0))$ (inverted triangle curve); (b) values of b at which the BHSCH growth rate matches the sharp interface growth rate at $k=1$. $\gamma = 0.04$ ($\bigcirc$ curve), $\gamma = 0.05$ (box curve).

C. Practical comparison between BHSCH and HSCH linear growth rates

In this section, we compare the linear growth rates for the BHSCH and HSCH models. Since we do not have an unstably stratified 1D equilibrium solution available for the HSCH model, we use simulations of the full equations of motion in the linear regime for both the BHSC and HSCH to determine the growth of perturbations from a 1D (flat) interface. Although we postpone a detailed discussion of our numerical algorithm until paper II,[2] we discuss a few relevant
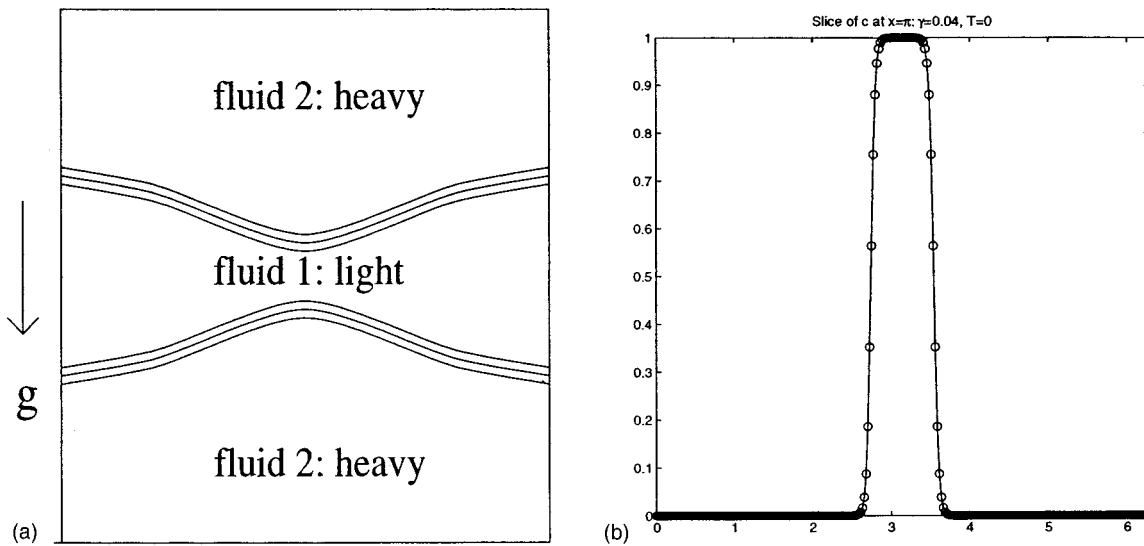
FIG. 7. Initial data for concentration (a) and its slice at $x=\pi$ (b) when $\gamma=0.05$.

features of the method here. The geometry we use is periodic in x and y ($\Omega=[0,2\pi]^2$) and in each periodic box, there are two interface layers rather than one as we have been considering up to now. Because of the periodicity, no boundary layers develop in the HSCH case. The initial interface positions are $(x,y_1(x,0))$ and $(x,y_2(x,0))$ where

$$y_1(x,0)=\pi-(0.5+\epsilon\cos(kx)),$$

$$y_2(x,0)=\pi+(0.5+\epsilon\cos(kx)),\quad 0\leqslant x\leqslant 2\pi,\quad (5.23)$$

and k denotes the wave number of the perturbation. The initial concentration field $c(x,y,0)=c_0(x,y)$ is given by

$$c_0(x,y)=\tfrac{1}{4}(1+\tanh((y-y_1(x))/(2\sqrt{(2*\mathbf{C}/\mathbf{D})})))*(1$$
$$-\tanh((y-y_2(x))/(2\sqrt{(2\mathbf{C}/\mathbf{D})}))).\quad (5.24)$$

The density of the BHSCH model is as before (5.12) and the density in the HSCH model is given by Eq. (2.24) with $\rho_2=1$ and $\alpha=0.1$ since relating α and α_g by

$$\alpha=\frac{\alpha_g}{1-\alpha_g}\quad (5.25)$$

matches $\rho(c)$ and $\tilde{\rho}(c)$ at $c=0$ and $c=1$. Thus, the initial data correspond to the situation of a light layer of fluid surrounded by a heavier one. See Fig. 7 for the $k=1$ initial data; the upper interface $(x,y_2(x,t))$ is unstable while the lower interface $(x,y_1(x,t))$ is stable.

In order to compare our results with those in the preceding section, we use the quartic free energy $f_0(c)$ from Eq. (4.5) in our simulations of the full HSCH and BHSCH models. Unlike the 1D equilibrium case, we encounter no difficulties in using the quartic free energy in the HSCH model. This is likely due to the periodic flow geometry. We find that the HSCH solution $c(\mathbf{x},t)$ typically lies within an $O(\gamma^2)$ neighborhood of [0, 1]. Additionally, we take $\mathbf{D}=4$ and $c_1=1$, $c_2=0$ and the parameters $\tilde{G}$, τ, η, $\mathbf{C}$ are the same as in the BHSCH case we considered previously. In the HSCH case, $\mathbf{M}$ is appropriately modified according to Eq. (3.2).

Because there are two interfaces, we note that even with $\epsilon=0$, the initial data $c_0(x,y)$ are only an approximation of the corresponding equilibrium solution for the BHSCH model and hence $c_0(x,y)$ is not an equilibrium solution for either model. In contrast, flat interfaces are equilibrium solutions of the sharp interface model.

To calculate the numerical approximation of the linear growth rates, we suppose at time t, the interface positions are given by

$$y_1(x,t)=\pi-(0.5+\epsilon\exp(\sigma_{1,k}t)\cos(kx)),$$

$$y_2(x,t)=\pi+(0.5+\epsilon\exp(\sigma_{2,k}t)\cos(kx)).$$

The growth rate of the unstable interface $\sigma_{2,k}$ is then computed by

$$\sigma_k=\frac{1}{T}\log((y_2(0,T)-(\pi+0.5))/\epsilon),\quad (5.26)$$

where we determine the position $y_2(0,T)$ using the height of the corresponding $c=0.5$ contour line at its intersection with the y-axis. We additionally use $\epsilon=0.05$ and $T=0.1$.

In Fig. 8, the growth rates $\sigma_{2,k}$ are shown for the BHSCH and HSCH models with $\mathbf{Pe}=1/\gamma$, $\mathbf{Pe}=1$, and $\gamma=0.05$. The BHSCH growth rates are denoted by $\bigcirc$ ($\mathbf{Pe}=1/\gamma$) and $\diamondsuit$ ($\mathbf{Pe}=1$). The HSCH growth rates are denoted by $+$ ($\mathbf{Pe}=1/\gamma$) and $\times$ ($\mathbf{Pe}=1$). For comparison, the sharp interface growth rate σ_0 (solid curve) is shown together with the BHSCH growth rates obtained in the preceding section: $\mathbf{Pe}=1/\gamma$ (dashed curve) and $\mathbf{Pe}=1$ (dotted–dashed curve). There are three main conclusions we draw from this figure. First, the BHSCH growth rates we calculate from the full equations and from the preceding section are consistent; there are slight differences but this is to be expected since the flow geometries are not the same. Second, the HSCH growth rates are consistently less than the BHSCH growth rates indicating more dissipation in the HSCH model. This is likely due to the fact that the initial data $c_0(x,y)$ is a better approximation of the BHSCH equilibrium than the HSCH equilib-
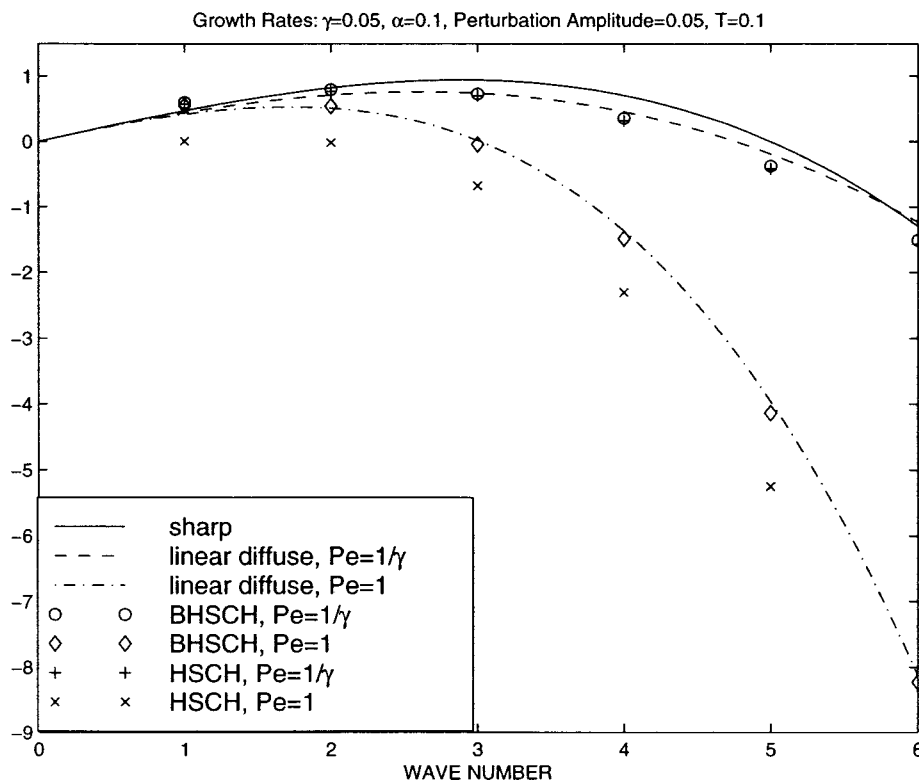
FIG. 8. A comparison of growth rates obtained from simulations of the full HSCH and BHSCH models (symbols) with those from the sharp interface and 1D BHSCH linear stability equations (5.17) and (5.18). Solid curve, sharp interface; dashed curve, 1D BHSCH growth rate with $\mathbf{Pe}=1/\gamma$, dotted–dashed curve, 1D BHSCH growth rate with $\mathbf{Pe}=1$; $\bigcirc$ curve, growth rate from full BHSCH model with $\mathbf{Pe}=1/\gamma$; diamond curve, growth rate from full BHSCH model with $\mathbf{Pe}=1$, $+$ curve, growth rate from full HSCH model with $\mathbf{Pe}=1/\gamma$; $\times$ curve, growth rate from full HSCH model with $\mathbf{Pe}=1$.

rium. Naturally, this effect is more pronounced at smaller $\mathbf{Pe}$ numbers. Third, in the $\mathbf{Pe}=1/\gamma$ case, the growth rates of the BHSCH and HSCH models are quite similar. This suggests that the analysis of the BHSCH linear growth rates we presented in the preceding section is relevant also to the HSCH model in periodic geometries.

VI. CONCLUSIONS

In this first paper of a two part series, the behavior of two model systems, to study binary fluid flow in a Hele-Shaw cell, is investigated. The equations are obtained using a simplification, for the Hele-Shaw setting, of a general system of equations describing the motion of a binary viscous fluid (NSCH equations[1]). This system takes into account the chemical diffusivity between different components of a fluid mixture and the extra fluid stresses induced by the inhomogeneity of the mixture (van der Waals type stresses[55]). In one of the models (HSCH), the binary fluid may be compressible due to diffusion. In the other model (BHSCH), a Boussinesq approximation is used and the binary fluid is incompressible.

The models are calibrated to yield the classical sharp interface model as a limiting case. The differences between the HSCH, BHSCH and sharp interface models are studied by considering equilibrium solutions and their linear stability. Somewhat surprisingly, the gravitational field actually affects the internal structure of the equilibrium transition layer and an equilibrium solution is obtained numerically only for the stably stratified case. Boundary layers in the equilibrium solution are observed and the evolution towards the stably stratified equilibrium simulated in one dimension.

The linear stability of unstably stratified equilibria is also analyzed. Linear convergence to the sharp interface growth

rates is observed in a parameter controlling the interface thickness. The BHSCH and HSCH growth rates are consistent although the HSCH system is seen to be slightly more diffusive than the BHSCH system. In addition, we identify the effect that each of the parameters, in the HSCH/BHSCH models, has on the linear growth rates. We then use this information to suggest a modified set of HSCH/BHSCH parameters for which a better match is obtained between the HSCH/BHSCH and sharp interface linear growth rates at finite interface thicknesses. This approach is quite general and has application beyond the current context. We suggest that agreement between the HSCH/BHSCH and sharp interface models may be improved by simply modifying the bond number by an amount approximately proportional to the interface thickness in order to match the sharp and BHSCH/HSCH growth rates at the most unstable wave number in the initial condition. There may be other, more optimal choices of parameters however. Evidence supporting our contention of improved agreement may be found in paper II.

In paper II,[2] we focus on the behavior of the models in the fully nonlinear regime through pinchoff and reconnection. To briefly preview that work, we find that the breakup of an unstably stratified fluid layer is smoothly captured by both models. Moreover, because the HSCH model is more diffusive than the BHSCH model, an earlier pinchoff time is predicted at finite interface thicknesses which causes subtle differences between the two in the pinchoff region. Away from the pinchoff region, both the HSCH and BHSCH models yield nearly identical results. At pinchoff, compressibility effects do not vanish in the sharp interface limit. This distinguishes the HSCH model from all others in which compressibility effects are neglected. It may turn out, for example,

that characterizing the limiting effect of compressibility at a topological transition may suggest a physically based selection mechanism for cutting and reconnecting sharp interfaces. In paper II, the effects of buoyancy, viscous, diffusional and surface tension forces are also investigated.

ACKNOWLEDGMENTS

[1] J. S. Lowengrub and L. Truskinovsky, "Quasi-incompressible Cahn–Hilliard fluids and topological transitions," Proc. R. Soc. London, Ser. A **454**, 2617 (1998).

[2] H.-G. Lee, J. S. Lowengrub, and J. Goodman, "Modeling pinchoff and reconnection in a Hele-Shaw cell. II. Analysis and simulation in the nonlinear regime," Phys. Fluids **14**, 514 (2002).

[3] J. S. Rowlinson and B. Widom, *Molecular Theory of Capillarity* (Clarendon, Oxford, 1979).

[4] H. S. Hele-Shaw, "The flow of water," Nature (London) **58**, 34 (1898).

[5] P. G. Saffman and G. I. Taylor, "The penetration of a fluid into a porous medium or Hele-Shaw cell containing a more viscous fluid," Proc. R. Soc. London, Ser. A **31**, 312 (1958).

[6] P. G. Saffman, "Viscous fingering in Hele-Shaw cells," J. Fluid Mech. **173**, 73 (1986).

[7] G. M. Homsy, "Viscous fingering in porous media," Annu. Rev. Fluid Mech. **19**, 271 (1987).

[8] P. Constantin, T. F. Dupont, R. E. Goldstein, L. P. Kadanoff, M. J. Shelley, and S.-M. Zhou, "Droplet breakup in a model of the Hele-Shaw cell," Phys. Rev. E **47**, 4169 (1993).

[9] T. F. Dupont, R. E. Goldstein, L. P. Kadanoff, and S.-M. Zhou, "Finite time singularity formation in Hele-Shaw systems," Phys. Rev. E **47**, 4182 (1993).

[10] R. Almgren, A. Bertozzi, and M. P. Brenner, "Stable and unstable singularities in the unforced Hele-Shaw cell," Phys. Fluids **8**, 1356 (1996).

[11] R. Goldstein, A. Pesci, and M. Shelley, "Attracting manifold for a viscous topology transition," Phys. Rev. Lett. **75**, 3665 (1995).

[12] R. Goldstein, A. Pesci, and M. Shelley, "Topology transitions and singularities in viscous flow," Phys. Rev. Lett. **70**, 3043 (1993).

[13] R. Goldstein, A. Pesci, and M. Shelley, "Instabilities and singularities in Hele-Shaw flow," Phys. Fluids **10**, 2701 (1998).

[14] R. Goldstein, A. Pesci, and M. Shelley, "Domain of convergence of perturbative solutions for Hele-Shaw flow near interface collapse," Phys. Fluids **11**, 2809 (1999).

[15] T. Hou, J. Lowengrub, and M. Shelley, "Removing the stiffness from interfacial flows with surface tension," J. Comput. Phys. **114**, 312 (1994).

[16] T. Hou, J. Lowengrub, and M. Shelley, "Boundary integral methods for multicomponent fluids and multiphase materials," J. Comput. Phys. **169**, 302 (2001).

[17] K. A. Gillow and S. D. Howison, http://www.maths.ox.ac.uk/howison/Hele-Shaw

[18] T. Hou, J. Lowengrub, and M. Shelley, "The long-time motion of vortex sheets with surface tension," Phys. Fluids **9**, 1933 (1997).

[19] C. S. Peskin and D. M. McQueen, "Numerical analysis of blood flow in the heart," J. Comput. Phys. **25**, 220 (1977).

[20] J. M. Hyman, "Numerical methods for tracking interfaces," Physica D **12**, 396 (1984).

[21] S. O. Unverdi and G. Tryggvason, "A front-tracking method for viscous, incompressible multi-fluid flows," J. Comput. Phys. **100**, 25 (1992).

[22] H. S. Udaykumar, M. M. Rao, and W. Shyy, "Eulerian-Lagrangian method for fluid flows with complex and moving boundaries," Int. J. Numer. Methods Fluids **22**, 691 (1996).

[23] N. Mansour and T. Lundgren, "Satellite formation in capillary jet breakup," Phys. Fluids A **2**, 1141 (1990).

[24] M. R. Nobari, Y.-J. Jan, and G. Tryggvason, "Head-on collision of drops—A numerical investigation," Phys. Fluids **8**, 29 (1996).

[25] C. S. Peskin and B. F. Prince, "Improved volume conservation in the computation of flows with immersed elastic boundaries," J. Comput. Phys. **105**, 33 (1993).

[26] R. Cortez and M. Minion, "The blob projection method for immersed boundary problems," J. Comput. Phys. **161**, 428 (2000).

[27] J. Eggers and T. F. Dupont, "Drop formation in a one dimensional approximation of the Navier–Stokes equations," J. Fluid Mech. **262**, 205 (1994).

[28] J. Eggers, "Theory of drop formation," Phys. Fluids **7**, 941 (1995).

[29] J. B. Keller and M. Miksis, "Surface tension driven flows," SIAM (Soc. Ind. Appl. Math.) J. Appl. Math. **43**, 268 (1983).

[30] J. Brackbill, D. B. Kothe, and C. Zemach, "A continuum method for modeling surface tension," J. Comput. Phys. **100**, 335 (1992).

[31] S. Osher and J. Sethian, "Fronts propagating with curvature dependent speed: algorithms based on Hamilton–Jacobi formulations," J. Comput. Phys. **79**, 12 (1988).

[32] Y. C. Chang, T. Y. Hou, B. Merriman, and S. Osher, "A level set formulation of Eulerian interface capturing methods for incompressible fluid flows," J. Comput. Phys. **124**, 449 (1996).

[33] M. Sussman, P. Smereka, and S. Osher, "A level set approach for computing solutions to incompressible two-phase flow," J. Comput. Phys. **114**, 146 (1994).

[34] M. Sussman and P. Smereka, "Axisymmetric free boundary problems," J. Fluid Mech. **341**, 269 (1997).

[35] M. Sussman, A. Almgren, J. Bell, P. Collela, L. Howell, and M. Welcome, "An adaptive level set approach for incompressible two-phase flows," J. Comput. Phys. **148**, 81 (1999).

[36] E. G. Puckett, A. Almgren, J. Bell, D. Marcus and W. Rider, "A high-order projection method for tracking fluid interfaces in variable density incompressible flows," J. Comput. Phys. **130**, 269 (1997).

[37] B. Lafaurie, C. Nardone, C. Scardoveli, S. Zaleski and G. Zanetti, "Modeling merging and fragmentation in multiphase flows with SURFER," J. Comput. Phys. **113**, 134 (1994).

[38] B. Nadiga and S. Zaleski, "Investigations of a two-phase fluid model," Eur. J. Mech. B/Fluids **15**, 885 (1996).

[39] R. Scardovelli and S. Zaleski, "Direct numerical simulation of free surface and interfacial flow," Annu. Rev. Fluid Mech. **31**, 567 (1999).

[40] D. Gueffier, J. Li, A. Nadim, R. Scardovelli, and S. Zaleski, "Volume of fluid interface tracking with smoothed surface stress methods for 3D flows," J. Comput. Phys. **152**, 423 (1999).

[41] R. Fedkiw, T. Aslam, B. Merriman, and S. Osher, "A nonoscillatory Eulerian approach to interfaces in multimaterial flows (the ghost fluid method)," J. Comput. Phys. **152**, 457 (1999).

[42] T. Y. Hou, Z. Li, S. Osher, and H. Zhao, "A hybrid method for moving interface problems with applications to Hele-Shaw flow," J. Comput. Phys. **134**, 236 (1997).

[43] B. T. Helenbrook, L. Martinelli, and C. K. Law, "A numerical method for solving incompressible flow problems with a surface of discontinuity," J. Comput. Phys. **148**, 366 (1999).

[44] J. Lowengrub, J. Goodman, H. Lee, E. Longmire, M. Shelley, and L. Truskinovsky, *Topological Transitions in Liquid/Liquid Interfaces* (Chapman & Hall/CRC Res. Notes Math., London, 1999), Vol. 409.

[45] P. C. Hohenberg and B. I. Halperin, "Theory of dynamic critical phenomena," Rev. Mod. Phys. **49**, 435 (1977).

[46] J. W. Cahn and J. E. Hilliard, "Free energy of a non-uniform system. I. Interfacial free energy," J. Chem. Phys. **28**, 688 (1958).

[47] V. N. Starovoitov, "Model of the motion of a two-component liquid with allowance of capillary forces," J. Appl. Mech. Tech. Phys. **35**, 891 (1994).

[48] M. E. Gurtin, D. Polignone, and J. Vinals, "Two-phase binary fluids and immiscible fluids described by an order parameter," Math. Methods Appl. Sci. **6**, 815 (1996).

[49] D. D. Joseph, "Fluid dynamics of two miscible liquids with diffusion and gradient stresses," Eur. J. Mech. B/Fluids **9**, 565 (1990).

[50] P. S. Perera and R. F. Sekerka, "Nonsolenoidal flow in a liquid diffusion couple," Phys. Fluids **9**, 376 (1997).

[51] L. K. Antanovskii, "A phase-field model of capillarity," Phys. Fluids **7**, 747 (1995).

[52] S. D. Poisson, *Nouvell Theorie de l'action Capillaire* (Bachelier, Paris, 1831).

[53] G. W. Gibbs, "On the equilibrium of heterogeneous substances," Trans.

Conn. Acad. Arts Sci. **3**, 108 (1876); **3**, 343 (1878). Reprinted in *The Scientific Papers of J. Willard Gibbs* (Longmans, Green, London, 1906), pp. 55–371.

[54] Lord Rayleigh, "On the theory of surface forces—II. Compressible fluids," Philos. Mag. **33**, 209 (1892).

[55] J. D. Van der Waals, "Therinodynamische theorie der kapillaritat unter voraussetzung stetiger dichteanderung," Z. Phys. Chem., Stoechiom. Verwandtschaftsl. **13**, 657 (1894); English translation in J. Stat. Phys. **20**, 197 (1979).

[56] D. J. Korteweg, "Sur la forme que prennent les equations du mouvements des fluides si l'on tient compte des forces capillaires causees par des variations de densite considerables mais continues et sur la theorie de la capillarite dans l'hypothese d'une variation continue de la densite," Arch. Neerl. Sci. Exactes Nat. Ser. II **6**, 1 (1901).

[57] H. T. Davis and L. E. Scriven, "Stress and structure of fluid interfaces," Adv. Chem. Phys. **49**, 357 (1982).

[58] D. Jacqmin, "Calculation of two-phase Navier–Stokes flows using phase-field modeling," J. Comput. Phys. **155**, 96 (1999).

[59] J. Hageman, M.S. thesis, Department of Aerospace and Mechanics, University of Minnesota, 1999.

[60] D. Jasnow and J. Vinals, "Coarse-grained description of thermocapillary flows," Phys. Fluids **8**, 660 (1996).

[61] M. Verschueren, Ph.D. thesis, Technische Universiteit Eindhoven, the Netherlands, 1999.

[62] R. Chella and J. Vinals, "Mixing of a two-phase fluid by cavity flow," Phys. Rev. E **53**, 3832 (1996).

[63] D. Jacqmin, "Contact line dynamics of a diffuse interface," J. Fluid Mech. **402**, 57 (2000).

[64] P. Seppecher, "Moving contact lines in the Cahn–Hilliard theory," Int. J. Eng. Sci. **34**, 977 (1996).

[65] F. Dell'Isola, H. Gouin, and G. Rotoli, "Radius and surface tension of microscopic bubbles by second gradient theory," Eur. J. Mech. B/Fluids **15**, 545 (1996).

[66] F. Dell'Isola, H. Gouin, and P. Seppecher, "Nucleation of spherical shell-like interfaces by second gradient theory: numerical simulations," C. R. Acad. Sci., Ser. IIa: Sci. Terre Planetes **320**, 211 (1995).

[67] D. Anderson and G. B. McFadden, "A diffuse-interface description of internal waves in a near critical fluid," Phys. Fluids **9**, 1870 (1997).

[68] L. de Sobrino, "Note on capillary waves in the gradient theory of interfaces," Can. J. Phys. **63**, 1132 (1985).

[69] L. de Sobrino and J. Peternelj, "On capillary waves in the gradient theory of interfaces," Can. J. Phys. **63**, 131 (1985).

[70] P. Galdi, D. D. Joseph, L. Preziosi, and S. Rionero, "Mathematical problems for miscible incompressible fluids with Korteweg stresses," Eur. J. Mech. B/Fluids **10**, 253 (1991).

[71] D. D. Joseph, A. Huang, and H. Hu, "Non-soleniodal velocity effects and Korteweg stresses in simple mixtures of incompressible liquids," Physica D **97**, 104 (1996).

[72] T. Y. Liao and D. D. Joseph, "Sidewall effects in the smoothing of an initial discontinuity," J. Fluid Mech. **342**, 37 (1997).

[73] D. Anderson, G. B. McFadden, and A. A. Wheeler, "Diffuse interface methods in fluid mechanics," Annu. Rev. Fluid Mech. **30**, 139 (1998).

[74] C.-W. Park and G. M. Homsy, "Two-phase displacement in Hele-Shaw cells: theory," J. Fluid Mech. **139**, 291 (1984).

[75] W. E and P. Palffy-Muhoray, "Phase separation in incompressible systems," Phys. Rev. E **55**, R3844 (1997).

[76] F. Otto and W. E, "Thermodynamically driven incompressible fluid mixtures," J. Chem. Phys. **107**, 10177 (1997).

[77] A. Shinozaki and Y. Oono, "Spinodal decomposition in a Hele-Shaw cell," Phys. Rev. A **45**, 2161 (1992).

[78] *On the Evolution of Phase Boundaries*, edited by M. Gurtin and G. B. McFadden, I.M.A. Series in Mathematics and its Applications 43 (Springer, New York, 1992).

[79] G. Caginalp, "Dynamics of conserved phase field system. Stefan-like, Hele-Shaw and Cahn–Hilliard models as asymptotic limits," IMA J. Appl. Math. **44**, 77 (1990).

[80] G. Caginalp and X. Chen, "Convergence of the phase field model to its sharp interface limits," Eur. J. Appl. Math. **9**, 417 (1998).

[81] R. L. Pego, "Front migration in the nonlinear Cahn–Hilliard equation," Proc. R. Soc. London, Ser. A **422**, 261 (1989).

[82] N. Alikakos, P. Bates, and X. Chen, "Convergence of the Cahn–Hilliard equations to the Hele-Shaw model," Arch. Ration. Mech. Anal. **128**, 165 (1994).

[83] R. Folch, J. Casademunt, A. Hernandez-Machado, and L. Ramirez-Piscina, "Phase-field model for Hele-Shaw flows with arbitrary viscosity contrast. I. Theoretical approach," Phys. Rev. E **60**, 1724 (1999); "Phase-field model for Hele-Shaw flows with arbitrary viscosity contrast. II. Numerical study," *ibid.* **60**, 1734 (1999).

[84] P. G. Saffman and G. I. Taylor, "The penetration of a fluid into a porous medium or Hele-Shaw cell containing a more viscous liquid," Proc. R. Soc. London, Ser. A **245**, 312 (1958).

[85] S. Allen and J. W. Cahn, "A microscopic theory for antiphase boundary motion and its application to antiphase domain coarsening," Acta Metall. **27**, 1084 (1979).

[86] P. Embid, J. B. Goodman, and A. Majda, "Multiple steady states for 1-d transonic flow," SIAM (Soc. Ind. Appl. Math.) J. Sci. Stat. Comput. **5**, 21 (1984).

[87] C. M. Elliot and S. Luckhaus, "A generalized diffusion equation for phase separation of a multi-component mixture with interfacial free energy," Institute for Math and Applications, Report No. 887, 1991.

[88] J. W. Cahn, "On spinodal decomposition," Acta Metall. **9**, 795 (1961).

[89] R. Braun, G. McFadden, and S. Coriell, "Morphological instability in phase-field models of solidification," Phys. Rev. E **49**, 4336 (1994).

[90] H. Keller, *Numerical Solution of Two Point Boundary Value Problems*, CBMS-NSF Regional Conference Series in Applied Mathematics, Vol. 24 (SIAM, Philadelphia, 1977).

[91] A. Karma and W.-J. Rappel, "Phase-field simulation of three dimensional dendrites: Is microscopic solvability theory correct?" J. Cryst. Growth **174**, 54 (1997).